

An MPC Method for Trajectory Tracking of Unmanned Vehicle with LMI-Constrained Unscented Kalman Filter

Renbo Qing, Xiaoming Tang, Hua Huang and Yongzhen Cao

Abstract—This paper investigates the model predictive control (MPC) for the trajectory tracking of the unmanned vehicle system with bounded disturbances and actuator saturation based on the unscented Kalman filter (UKF). In order to obtain accurate system state, the linear matrix inequality (LMI)-constrained UKF is addressed by solving the LMI optimization problem. Moreover, by expressing the saturating linear feedback law as convex hull and describing the stability of the vehicle kinematics model with bounded disturbance via the quadratic bounded theorem, a model predictive controller to achieve trajectory tracking is proposed by solving the infinite horizon optimization problem. The effectiveness of the proposed approach is verified by the co-simulation platform of Matlab/Simulink and Carsim. The results of simulations show that this approach can improve the accuracy of state estimation as well as the trajectory tracking control.

Index Terms—unscented Kalman filter, trajectory tracking, model predictive control, linear matrix inequality.

I. INTRODUCTION

IT is undoubtedly that the unmanned vehicle technology has a great impact on the transportation and logistics industry. With the continuous development of core technologies, such as artificial intelligence and sensor detection, unmanned vehicle technology is also constantly updating [1–7]. Generally, unmanned vehicle technology includes environmental perception, path planning, and trajectory tracking. Among them, trajectory tracking is one of the key issues and the primary prerequisite for unmanned vehicles to complete work tasks [8–12].

As everyone knows, the tracking performance of unmanned vehicle depends not only on the tracking control algorithm, but also on the accuracy of the vehicle state estimation. Kalman filter (KF) is extensively used in state estimation due to the strong anti-interference performance, simple programming, small memory footprint, fast operation speed, and a large number of literatures can be found in studying the KF [13–17]. It should be noticed that filtering is great challenging due to the nonlinearity which becomes a

hot research topic in the last decades. Among the existing approaches for addressing the problem of nonlinearity [18–22], UKF [21] and extended KF (EKF) [22] demonstrate great advantage, since they take Taylor's theorem and unscented transformation to linearize the system and the fruitful of theories of linear system can be directly utilized. For instance, [23] proposed an estimation scheme based on dual EKF technology, the first EKF was used for estimating the vehicle state, and the second EKF was used for estimating the vehicle parameters. In [24], the estimation of the rapidly varying handling state vector with EKF was investigated. In [25], the adaptive cubature KF (ACKF) was used for estimating the system state, and the adaptive law was used to eliminate the influence of unknown interference. Reference [26] presented a scheme of region-level instance segmentation and EKF. In addition, other types of Kalman filters have been proposed in the framework of nonlinear systems, see e.g., [27–29]. In [27], the error state KF was proposed to estimate localization position and vehicle state. In [28], a two-layer control scheme was proposed, the outer layer consisted of a trajectory tracking controller, and the inner layer included a zonotopic KF. Additionally, a consensus-extended KF was designed in [29]. However, the above works are all focused on the influence of noise on filtering results, which ignored the state constraints of system. Hence, a great many of papers start to investigate the Kalman filters with constraints [30–33]. In [30], a disturbance observer based on state-constrained KF was proposed to estimate the vehicle state. In [31], a constrained UKF algorithm was subsequently introduced to estimate the tire-road friction coefficient, aiming to improve the convergence speed and estimation accuracy. Based on accelerometer, gyroscope and wheel speed, a constrained EKF was explored in [32]. Reference [33] provided a double-stage KF estimation strategy consisting of complementary KF and multi-state observation-constrained KF. Reference [34] proposed a linearly constrained EKF approach to solve the problems of model mismatch and unknown noise. However, to the best of the authors' knowledge, few studies have expressed the state estimation as an optimization problem in the form of LMI when considering the KF method.

Recently, MPC has becomes one of the most popular tracking control algorithms in unmanned vehicle technology, since it possesses the unique feature of dealing with the physical constraints in unmanned vehicle systems, see, e.g., [35–39]. Reference [35] proposed a path following model predictive controller that considered model mismatch. A novel approach of combining lane detection and MPC approach was presented in [36] to maintain the accuracy and stability of trajectory tracking control for unmanned

Manuscript received October 9, 2023; revised February 26, 2024.

Renbo Qing is a graduate student of Chongqing University of Posts and Telecommunications, Chongqing 400065, China (e-mail:15023759434@163.com).

Xiaoming Tang is a professor of Information Physics System Theory and Application Research Team, Chongqing University of Posts and Telecommunications, Chongqing 400065, China; (corresponding author to provide e-mail: txmmyeye@126.com).

Hua Huang is a graduate student of Chongqing University of Posts and Telecommunications, Chongqing 400065, China (e-mail:hh_breeze@126.com).

Yongzhen Cao is a graduate student of Chongqing University of Posts and Telecommunications, Chongqing 400065, China (e-mail:caoyongzhenovo@126.com).

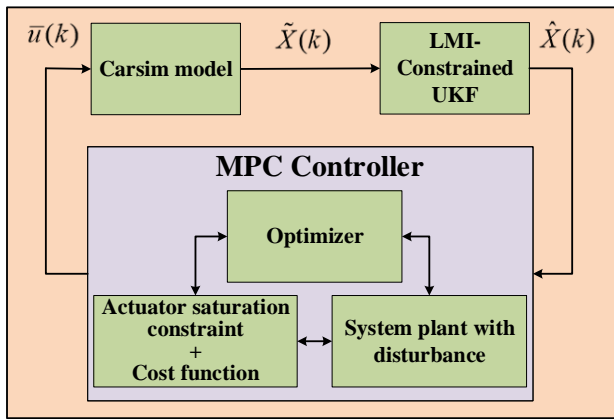


Fig. 1. The overall framework considered in this paper including: model, filter and controller

vehicle system. A nonlinear model predictive controller was designed in [37], which considered both hard and softened constraints. Reference [38] investigated an MPC approach with finite time horizon, which considered the time-varying and uncertain parameters, as well as the external disturbance. Reference [39] proposed a control scheme of MPC and Robust control. The model predictive controller solved the problem of trajectory tracking and trajectory planning, and the robust controller tracked the phase trajectory to ensure the stability of the motion. However, it is worth noting that the above studies are under a common assumption that the system states are measurable. In fact, it is hard to directly obtain the system state in practical applications. Therefore, the state observer is usually used in MPC method to obtain system state. In [40–43], the state of unmanned vehicle system was estimated based on its measurable signal which was served as the input of the model predictive controller. In [40], a composite control scheme composed of disturbance observer and nonlinear MPC was devised to improve the control performance of underwater vehicle system with disturbance, model mismatch, and input saturation. In [41], an MPC method combined with extended state observer was proposed, which considered the speed information loss, dynamic uncertainty and disturbance. In [42], an UKF combined with multi-constraints MPC strategy was proposed, where UKF was based on a magic formula tire model. In [43], a four-degree-of-freedom vehicle model and an UKF were addressed to estimate the vehicle state, and model predictive controller was designed to achieve real-time control based on the estimated state of the vehicle. However, limited works focus on the combination of LMI-constrained UKF and MPC approach, not to mention the actuator saturation and external disturbance, which prompts the further study in this paper.

In this paper, an infinite horizon model predictive controller is designed for the trajectory tracking problem of unmanned vehicle system based on the LMI-constrained UKF method which explicitly considers the actuator saturation and bounded disturbance. According to the vehicle dynamics model, the UKF with constraints is presented by solving the LMI optimization problem to get the estimation state required by the controller. According to the vehicle kinematics model, the model predictive controller is proposed

by considering system disturbance and actuator saturation, which are handled via the quadratic bounded theorem and the convex hull expression, respectively. The structure of the approach as seen in Fig. 1. According to the vehicle model provided by Carsim, the vehicle state is obtained through UKF which is served as the input of the controller. In model predictive controller, the infinite horizon cost function is optimized online by using LMI technology to obtain control input for vehicle, which explicitly considers the bounded disturbance and actuator saturation simultaneously.

The organization of the paper is as below: Section II provides the vehicle model, and Section III focuses on LMI-constrained UKF. Section IV introduces a robust model predictive controller. Simulation and discussion of results are presented in V. The conclusion is given in Section Section VI.

II. VEHICLE MODELING

A. Vehicle Dynamics Model

In this section, we establish the vehicle dynamics model, as shown in Fig. 2. We assume certain conditions for analyzing the front-wheel-drive unmanned vehicle. These assumptions include operation on a level road, disregard for vertical motion effects, neglecting the longitudinal and lateral coupling relationships of tire forces, and ignoring any lateral movement of the vertical load [44]. The resulting equations are presented as follows

$$m\ddot{x} = m\dot{y}\dot{\varphi} + 2(F_{xf} + F_{xr}) \quad (1)$$

$$m\ddot{y} = -m\dot{x}\dot{\varphi} + 2(F_{yf} + F_{yr}) \quad (2)$$

$$I_z\ddot{\varphi} = 2(aF_{yf} - bF_{yr}) \quad (3)$$

where m represents the mass of the vehicle; the yaw angle φ is defined as the angle between x axis and X axis, with counterclockwise rotation considered as positive; F_{xf} and F_{xr} indicate the forces exerted on the front and rear tires along the x -axis, F_{yf} and F_{yr} signify the forces on the front and rear tires along the y -axis; I_z denotes the moment of inertia of the vehicle about the z -axis; a and b correspond to the distances from the vehicle's center of mass to the front and rear axles.

The conversion relationship between the resultant force in the x and y directions and the longitudinal and lateral forces are as follows

$$F_{xr} = F_{lr}\cos\delta_r - F_{cr}\sin\delta_r \quad (4)$$

$$F_{xf} = F_{lf}\cos\delta_f - F_{cf}\sin\delta_f \quad (5)$$

$$F_{yr} = F_{lr}\sin\delta_r + F_{cr}\cos\delta_r \quad (6)$$

$$F_{yf} = F_{lf}\sin\delta_f + F_{cf}\cos\delta_f \quad (7)$$

where F_{lr} and F_{cr} imply the force on rear tire in the longitudinal and lateral direction, F_{lf} and F_{cf} denote the force on the front tire in the longitudinal and lateral direction, the computation of the above parameters is referenced in [44]; δ_f and δ_r are the wheel deflection.

According to the conversion relationship between the vehicle body coordinate system and the inertial coordinate system

$$\dot{Y} = \dot{x}\sin\varphi + \dot{y}\cos\varphi \quad (8)$$

$$\dot{X} = \dot{x}\cos\varphi - \dot{y}\sin\varphi \quad (9)$$

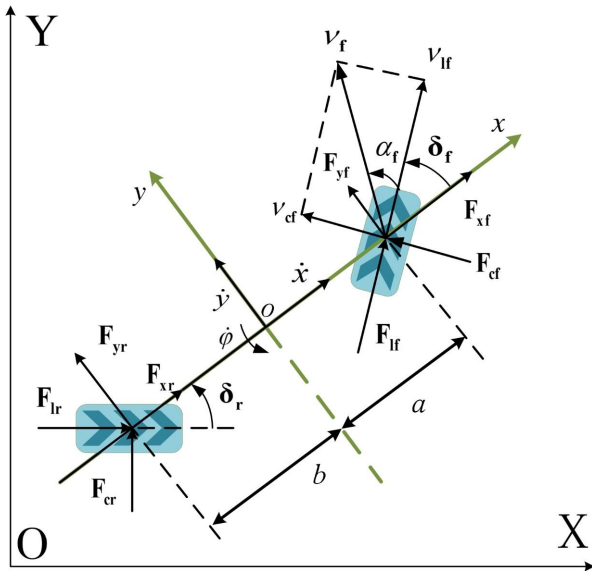


Fig. 2. Vehicle monorail model for vehicle dynamics

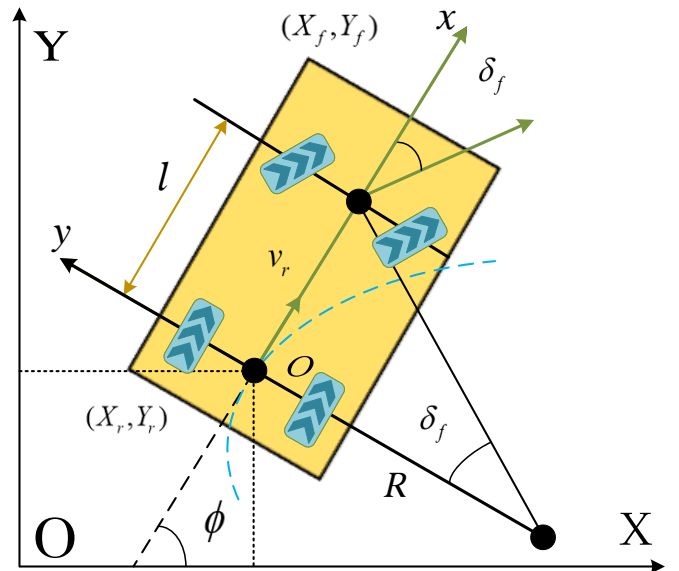


Fig. 3. The vehicle kinematics model

The vehicle nonlinear dynamics model can be obtained through equation (1) to equation (9) as follows

$$\dot{\tilde{X}} = f(\tilde{X}, \tilde{u}) \quad (10)$$

where $\tilde{X} = [\dot{y} \ \dot{x} \ \varphi \ \dot{\varphi} \ Y \ X]^T$, $\tilde{u} = \delta_f$.

B. Vehicle Kinematics Model

Fig. 3 shows the kinematics model of vehicle. The vehicle kinematics equations are as follows

$$\begin{bmatrix} \dot{X} \\ \dot{Y} \\ \dot{\varphi} \end{bmatrix} = \begin{bmatrix} \cos\varphi \\ \sin\varphi \\ \tan\delta/l \end{bmatrix} v \quad (11)$$

Equation (11) can be described as

$$\dot{\xi} = \mathcal{F}(\xi, u) \quad (12)$$

where $\xi = [X \ Y \ \varphi]^T$, $u = [v \ \delta]^T$.

For a specified reference trajectory, it can be described by the vehicle's motion path. Every point along this trajectory complies with equation (12), the subscript *ref* is employed to denote the reference point, which is generally in the form of

$$\dot{\xi}_{ref} = \mathcal{F}(\xi_{ref}, u_{ref}) \quad (13)$$

where ξ_{ref} and u_{ref} are respectively defined as $\xi_{ref} = [X_{ref} \ Y_{ref} \ \varphi_{ref}]^T$, $u_{ref} = [v_{ref} \ \delta_{ref}]^T$.

Through Taylor theorem and Euler discretization, we can get

$$\bar{X}_{k+1} = A_k \bar{X}_k + B_k \bar{u}_k \quad (14)$$

with

$$A_k = \begin{bmatrix} 1 & 0 & -v_{ref} \sin\varphi_{ref} T \\ 0 & 1 & v_{ref} \cos\varphi_{ref} T \\ 0 & 0 & 1 \end{bmatrix} \quad (15)$$

$$B_k = \begin{bmatrix} \cos\varphi_{ref} T & 0 \\ \sin\varphi_{ref} T & 0 \\ \frac{\tan\delta_{ref} T}{l} & \frac{v_{ref} T}{l \cos^2\delta_{ref}} \end{bmatrix}$$

where \bar{X}_k is the result of $\xi - \xi_{ref}$ discretization, T is the sampling time.

III. STATE ESTIMATION

A. UKF for State Estimation

System equation (10) is selected for state estimation, and considers process noise and measurement noise.

$$\begin{cases} \dot{\tilde{X}} = f(\tilde{X}, \tilde{u}) + q \\ \tilde{y} = h(\tilde{X}) + r \end{cases} \quad (16)$$

where $q \sim N(0, Q_k)$, $\tilde{y} = h(\tilde{X}) = [X, Y, \varphi]$, $r \sim N(0, R_k)$.

(1) Prediction step. Calculate the sigma sampling of posterior probability distribution, .

$$\mathcal{X}_{k-1}^{+(i)} = \begin{cases} \hat{x}_{k-1}, & i = 0 \\ \hat{x}_{k-1} + (\sqrt{(n+\lambda)P_{k-1}})^{(i-1)}, & i = 1, 2, \dots, n \\ \hat{x}_{k-1} - (\sqrt{(n+\lambda)P_{k-1}})^{(i-n-1)}, & i = n+1, \dots, 2n \end{cases} \quad (17)$$

where $\lambda = \alpha^2(n+k) - n$, α and k are the proportional parameters, the matrix P_{k-1} is computed using the provided initial values and the expression for P_k in equation (24).

Then, the nonlinear transformation

$$\mathcal{X}_k^{-*(i)} = f(\mathcal{X}_{k-1}^{+(i)}, u_k), \quad i = 0, 1, \dots, 2n \quad (18)$$

The prior probability distribution of the state \hat{x}_k^- and the error covariance $P_k^- = E[e_k^-(e_k^-)^T]$ are computed.

$$\hat{x}_k^- = \sum_{i=0}^{i=2n} \mathcal{W}_m^{(i)} \mathcal{X}_k^{-*(i)}, \quad (19)$$

$$P_k^- = \sum_{i=0}^{i=2n} \mathcal{W}_c^{(i)} [\mathcal{X}_k^{-*(i)} - \hat{x}_k^-][\mathcal{X}_k^{-*(i)} - \hat{x}_k^-]^T + Q_k$$

where $e_k^- = x_k - \hat{x}_k^-$.

Compute the weights

$$\begin{aligned} \mathcal{W}_m^{(0)} &= \frac{\lambda}{n + \lambda}, \\ \mathcal{W}_c^{(0)} &= \frac{\lambda}{n + \lambda} + 1 - \alpha^2 + \beta, \\ \mathcal{W}_m^{(i)} &= \mathcal{W}_c^{(i)} = \frac{1}{2(n + \lambda)}, \quad i = 1, 2, \dots, 2n \end{aligned} \quad (20)$$

where β is used to introduce the high-order moment information.

(2) **Update step.** Similarly, compute the sigma points

$$\mathcal{X}_k^{-(i)} = \begin{cases} \hat{x}_k^-, & i = 0 \\ \hat{x}_k^- + (\sqrt{(n + \lambda)P_k^-})^{(i-1)}, & i = 1, 2, \dots, n \\ \hat{x}_k^- - (\sqrt{(n + \lambda)P_k^-})^{(i-n-1)}, & i = n + 1, \dots, 2n \end{cases} \quad (21)$$

Next, the nonlinear transformation

$$\mathcal{Z}_k^{(i)} = h(\mathcal{X}_k^{-(i)}), \quad i = 0, 1, \dots, 2n \quad (22)$$

Finally, compute the mean predicted measurement z_k , predicted measurement error covariance P_z and cross error covariance $P_{xz} = E[e_k^- \rho_k^T]$

$$\begin{aligned} z_k &= \sum_{i=0}^{i=2n} \mathcal{W}_m^{(i)} \mathcal{Z}_k^{(i)}, \\ P_z &= \sum_{i=0}^{i=2n} \mathcal{W}_c^{(i)} [\mathcal{Z}_k^{(i)} - z_k][\mathcal{Z}_k^{(i)} - z_k]^T + R_k, \\ P_{xz} &= \sum_{i=0}^{i=2n} \mathcal{W}_c^{(i)} [\mathcal{X}_k^{-(i)} - \hat{x}_k^-][\mathcal{Z}_k^{(i)} - z_k]^T \end{aligned} \quad (23)$$

where $\rho_k = y_k - z_k$, which y_k is the observed value.

The gain K_k , state mean \hat{x}_k and covariance P_k are computed by follows.

$$\begin{aligned} K_k &= P_{xz} P_z^{-1}, \\ \hat{x}_k &= \hat{x}_k^- + K_k \rho_k, \\ P_k &= P_k^- - K_k P_z K_k^T \end{aligned} \quad (24)$$

B. LMI Formulation of the UKF

The state estimation is essentially an optimization problem, we can use LMI technology to solve the following optimization problem, the gain K_k is selected to minimize the objective function [45]

$$\begin{aligned} J_k &= \frac{1}{2} [(\rho_k - H_k K_k \rho_k)^T R_k^{-1} (\rho_k - H_k K_k \rho_k) \\ &\quad + (K_k \rho_k)^T (P_k^-)^{-1} (K_k \rho_k)] \end{aligned} \quad (25)$$

By considering $\rho_k = H_k e_k^- + v_k$, we get

$$H_k = P_{xz}^T (P_k^-)^{-1} \quad (26)$$

Combining equation (25) and equation (26), we have

$$\begin{aligned} J_k &= \frac{1}{2} \rho_k^T [(1 - P_{xz}^T (P_k^-)^{-1} P_{xz} P_z^{-1})^T R_k^{-1} \\ &\quad \times (1 - P_{xz}^T (P_k^-)^{-1} P_{xz} P_z^{-1}) \\ &\quad + (P_{xz} P_z^{-1})^T (P_k^-)^{-1} P_{xz} P_z^{-1}] \rho_k \end{aligned} \quad (27)$$

The cost function is selected as follows

$$J_k(Z_k) = \frac{1}{2} \rho_k^T Z_k \rho_k \quad (28)$$

where Z_k is subject to the constraint

$$\begin{aligned} Z_k &\geq (1 - P_{xz}^T (P_k^-)^{-1} P_{xz} P_z^{-1})^T R_k^{-1} \\ &\quad \times (1 - P_{xz}^T (P_k^-)^{-1} P_{xz} P_z^{-1}) \\ &\quad + (P_{xz} P_z^{-1})^T (P_k^-)^{-1} P_{xz} P_z^{-1} \end{aligned} \quad (29)$$

Use the Schur complement lemma, equation (29) is equivalent to

$$\begin{aligned} \begin{bmatrix} Z_k & * & * \\ \Theta & R_k & * \\ \Psi & 0 & P_z^{-1} \end{bmatrix} &\geq 0, \\ \Theta &= (1 - P_{xz}^T (P_k^-)^{-1} P_{xz} B_k), \Psi = P_{xz} B_k \end{aligned} \quad (30)$$

where the design variable is chosen to be $B_k = P_z^{-1}$. In the unconstrained case, minimizing equation (28) over all possible Z_k and B_k subject to $Z_k = Z_k^T > 0$, $B_k = B_k^T > 0$ and equation (30) yields the optimal gain $K_k = P_{xz} B_k = P_{xz} P_z^{-1}$. In some cases, the additional information of system state and environment can be incorporated into the optimization problem in the form of LMI.

$$\begin{bmatrix} d^2 & \hat{x}_k^T \\ \hat{x}_k & D_k^{-1} \end{bmatrix} \geq 0 \quad (31)$$

where $D_k = D_k^T > 0$.

IV. DESIGN OF MODEL PREDICTIVE CONTROLLER

In this section, a robust model predictive controller is introduced. According to above vehicle kinematics model, the system can be described as

$$\begin{aligned} \hat{X}_{k+1} &= A_k \hat{X}_k + B_k \text{sat}(\bar{u}_k) + w_k \\ [A_k \quad B_k] &\in \Omega \end{aligned} \quad (32)$$

where $\hat{X}_k = \xi_e - \xi_{ref}$, ξ_e is obtained by LMI-constrained UKF, and $\Omega = Co\{[A_1 \quad B_1], \dots, [A_L \quad B_L]\}$. The function $\text{sat} : \mathbb{R}^{n_u} \rightarrow \mathbb{R}^{n_u}$ is the standard saturation function, defined as $\text{sat}(\bar{u}_k) = [\text{sat}(\bar{u}_1), \text{sat}(\bar{u}_2), \dots, \text{sat}(\bar{u}_{n_u})]^T$, and $\text{sat}(\bar{u}_k) = \text{sign}(u_k) \min\{|\bar{u}_k|, \bar{u}_{max}\}$. The w_k satisfies $\|w_k\| \leq 1$ for all $k \geq 0$.

For any time-varying A_k and B_k , $[A_k \quad B_k] \in \Omega$ implies that

$$[A_k \quad B_k] = \sum_{i=1}^L \lambda_i [A_i \quad B_i] \quad (33)$$

where $\lambda_i \geq 0$, $\sum_{i=1}^L \lambda_i = 1$, $i = 1, \dots, L$.

Lemma 1: [46] Suppose that $P \in \mathbb{R}^{n_x \times n_x}$, $P > 0$, and let an ellipsoid $\Omega_p = \{x | x^T P x \leq 1\}$ and a polyhedron of auxiliary matrix F , $\mathcal{L}(F) = \{x \in \mathbb{R}^{n_x} : |f_l^T x| \leq 1, l = 1, 2, \dots, n_u\}$, $\Omega_p \subset \mathcal{L}(F)$ if and only if: $f_l^T P^{-1} f_l \leq 1, l = 1, 2, \dots, n_u$, where f_l^T is the l th row of F .

Let \mathcal{V} is a set of $n_u \times n_u$ diagonal matrices, and the elements taking values on 0 or 1. V_s and $V_s^- = I - V_s$ are the element of \mathcal{V} , which $s \in \{1, 2, \dots, 2^{n_u}\}$.

Lemma 2: [47] Let $F, H \in \mathbb{R}^{n_u \times n_u}$ be known. If $|h_l^T x| \leq 1$ for all $l = 1, 2, \dots, n_u$, then

$$\text{sat}(F x) \in Co\{V_s F x + V_s^- H x\} \quad (34)$$

where $s \in [1, 2^{n_u}]$.

Lemma 3: [48] For any allowable $w_{k+j}, j \geq 0$, the system equation (32) is quadratically bounded if the following conditions are satisfied.

1) P is a common Lyapunov matrix.

2) $\hat{X}_k^T P \hat{X}_k \geq 1$ implies that $\hat{X}_{k+1}^T P \hat{X}_{k+1} \leq \hat{X}_k^T P \hat{X}_k$.

3) the ellipsoid $\varepsilon_P = \{\hat{X}_k | \hat{X}_k^T P \hat{X}_k \leq 1\}$ is a robustly positively invariant set.

By applying Lemma 1 and Lemma 2, $\text{sat}(\bar{u}_k)$ can be described as

$$\text{sat}(\bar{u}_k) = \hat{F} \hat{X}_k \quad (35)$$

where $\hat{F} = \sum_{i=1}^L \sum_{s=1}^{2^{n_u}} \lambda_i \eta_s \bar{F}_i$, $\bar{F}_i = (V_s F + V_s^- H)$, $\eta_s \geq 0$, $\sum_{s=1}^{2^{n_u}} \eta_s = 1$.

We propose the ‘‘min-max’’ optimization problem in the infinite horizon to design the controller.

$$\begin{aligned} & \min_{\text{sat}(\bar{u}_k)} \max_{[A_k \ B_k] \in \Omega, i \geq 0} J_\infty(k) \\ J_\infty(k) &= \sum_{j=0}^{\infty} [\hat{X}_{k+j|k}^T Q_c \hat{X}_{k+j|k} + \text{sat}(\bar{u}_{k+j|k})^T R_c \text{sat}(\bar{u}_{k+j|k})] \end{aligned} \quad (36)$$

where $Q_c > 0$ and $R_c > 0$ are proper weighting matrices.

Theorem 1: Assume that $\hat{X}_k = \hat{X}_{k|k}$ represents the state of system equation (32) at the sampling time k . The ellipsoid $\Omega_p = \{\hat{X}_{k|k} | \hat{X}_{k|k}^T Q^{-1} \hat{X}_{k|k} \leq 1\}$ is an invariant set of the closed-loop system under the state feedback control law equation (35). For any $\hat{X}_{k|k} \in \Omega_p$, if the following conditions are satisfied,

$$\begin{bmatrix} I & * \\ \hat{X}_{k|k} & Q \end{bmatrix} \geq 0 \quad (37)$$

$$\begin{bmatrix} (1-\tau)Q & * & * & * & * \\ 0 & \gamma\tau I & * & * & * \\ A_i Q + B_i(V_s Y + V_s^- Z) & \gamma I & Q & * & * \\ Q_c^{\frac{1}{2}} Q & 0 & 0 & \gamma I & * \\ R_c^{\frac{1}{2}}(V_s Y + V_s^- Z) & 0 & 0 & 0 & \gamma I \end{bmatrix} \geq 0 \quad (38)$$

$$\begin{bmatrix} I & * \\ z_l & Q \end{bmatrix} \geq 0, \quad z_l = h_l Q \quad (39)$$

there exists the control law given by $F = YQ^{-1}$, $H = ZQ^{-1}$ that minimizes the upper bound $V(\hat{X}_{k|k})$ of the objective function at the sampling time K .

Proof: Select a Lyapunov function as $V(\hat{X}_{k+j|k}) = \hat{X}_{k+j|k}^T P \hat{X}_{k+j|k}$, $j \geq 0$. Assume $\Delta V(\hat{X}_{k+j|k})$ satisfy

$$\begin{aligned} & \Delta V(\hat{X}_{k+j|k}) \\ &= V(\hat{X}_{k+j+1|k}) - V(\hat{X}_{k+j|k}) \\ &\leq -[\hat{X}_{k+j|k}^T Q_c \hat{X}_{k+j|k} + \text{sat}(u_{k+j|k})^T R_c \text{sat}(u_{k+j|k})] \end{aligned} \quad (40)$$

the system is stable, and equation (40) is the stability condition of the system.

Applying Lemma 3, we can obtain the formula that holds equation (40)

$$\begin{aligned} & \hat{X}_{k+j|k}^T P \hat{X}_{k+j|k} - w_k^T w_k \geq 0 \\ & \Downarrow \\ & \hat{X}_{k+j|k}^T P \hat{X}_{k+j|k} - \hat{X}_{k+j+1|k}^T P \hat{X}_{k+j+1|k} - [\hat{X}_{k+j|k}^T \\ & \times Q_c \hat{X}_{k+j|k} + \text{sat}(u_{k+j|k})^T R_c \text{sat}(u_{k+j|k})] \geq 0 \end{aligned} \quad (41)$$

Applying the S-procedure theory to equation (41) reveals the existence of a parameter, denoted as τ , yielding the following equation

$$\begin{aligned} & \hat{X}_{k+j|k}^T P \hat{X}_{k+j|k} - \hat{X}_{k+j+1|k}^T P \hat{X}_{k+j+1|k} \\ & - \hat{X}_{k+j|k}^T Q_c \hat{X}_{k+j|k} - \text{sat}(u_{k+j|k})^T R_c \text{sat}(u_{k+j|k}) \\ & - \tau(\hat{X}_{k+j|k}^T P \hat{X}_{k+j|k} - w_k^T w_k) \geq 0 \end{aligned} \quad (42)$$

Then, let $P = \gamma Q^{-1}$ and rewrite equation (42) into matrix form as follows

$$\begin{bmatrix} \hat{X}_{k+j|k} \\ w_k \end{bmatrix}^T \left\{ \begin{bmatrix} \Theta & 0 \\ 0 & \frac{1}{\gamma} \tau \end{bmatrix} - [\hat{A}_i \ I]^T Q^{-1} [\hat{A}_i \ I] \right\} \begin{bmatrix} \hat{X}_{k+j|k} \\ w_k \end{bmatrix} \geq 0 \quad (43)$$

where $\Theta = (1-\tau)Q^{-1} - \frac{1}{\gamma}Q_c - \frac{1}{\gamma}\bar{F}_i^T R_c \bar{F}_i$, $\hat{A}_i = A_i + B_i \bar{F}_i$. Equation (43) is equivalent to

$$\begin{bmatrix} \Theta & 0 \\ 0 & \frac{1}{\gamma} \tau \end{bmatrix} - [\hat{A}_i \ I]^T Q^{-1} [\hat{A}_i \ I] \geq 0 \quad (44)$$

Using Schur complement lemma for equation (44), we get

$$\begin{bmatrix} (1-\tau)Q^{-1} & * & * & * & * \\ 0 & \frac{1}{\gamma} \tau I & * & * & * \\ A_i + B_i \bar{F}_i & I & Q & * & * \\ Q_c^{\frac{1}{2}} & 0 & 0 & \gamma I & * \\ R_c^{\frac{1}{2}} \bar{F}_i & 0 & 0 & 0 & \gamma I \end{bmatrix} \geq 0 \quad (45)$$

Multiply $\text{diag}\{Q \ I \ I \ I \ I\}$ and $\text{diag}\{I \ \gamma \ I \ I \ I\}$ on the left and right sides of equation (45), respectively. Let $Y = FQ$, and $Z = HQ$, if $z_l^T Q^{-1} z_l \leq 1$ holds, we obtain

$$\begin{bmatrix} (1-\tau)Q & * & * & * & * \\ 0 & \gamma\tau I & * & * & * \\ A_i Q + B_i(V_s Y + V_s^- Z) & \gamma I & Q & * & * \\ Q_c^{\frac{1}{2}} Q & 0 & 0 & \gamma I & * \\ R_c^{\frac{1}{2}}(V_s Y + V_s^- Z) & 0 & 0 & 0 & \gamma I \end{bmatrix} \geq 0 \quad (46)$$

where τ is pre-specify.

If equation (46) holds, then equation (40) holds, the system stability condition $\Delta V(\hat{X}_{k+j|k}) \leq 0$ is included in equation (40). For any $\hat{X}_{k|k} \in \Omega_p$, adding equation (40) from $j = 0$ to $j = \infty$, we get

$$\max_{[A_k \ B_k] \in \Omega, \hat{X}_{k|k} \in \Omega_p} J_\infty(k) \leq \gamma \quad (47)$$

Then, using Schur complement lemma, condition $z_l^T Q^{-1} z_l \leq 1$ and $\hat{X}_k^T Q^{-1} \hat{X}_k \leq 1$ are equivalent into

$$z_l^T Q^{-1} z_l \leq 1 \iff \begin{bmatrix} I & * \\ z_l & Q \end{bmatrix} \geq 0 \quad (48)$$

$$\hat{X}_k^T Q^{-1} \hat{X}_k \leq 1 \iff \begin{bmatrix} I & * \\ \hat{X}_k & Q \end{bmatrix} \geq 0 \quad (49)$$

End of proof.

According to Theorem 1, we propose the following optimization problem to design the control law to minimize the upper bound of equation (47).

$$\begin{aligned} & \min_{\gamma, Q, Y, Z} \gamma \\ & \text{s.t. Equations. (46), (48) and (49)} \end{aligned} \quad (50)$$

V. SIMULATION RESULTS

The effectiveness of the methods proposed in Section III and Section IV are verified through the vehicle simulation model provided by Carsim in the co-simulation platform of Matlab/Simulink and Carsim, as shown in Fig. 4.

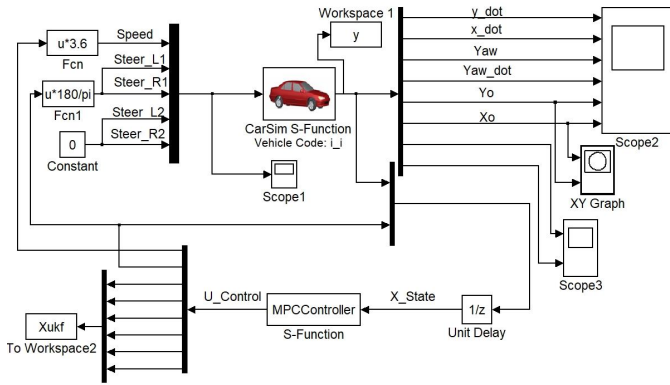


Fig. 4. The co-simulation platform of Simulink and Carsim.

The initial position of unmanned vehicle is $\hat{X}(0) = [0 \ 0 \ 0]^T$. Let $T = 0.1$ second, $l = 2.6$ m and $\delta_f(0) = 0.104$ rad, we can get

$$d = 4, R_c = 0.1, \bar{u}_{max} = 0.436$$

and

$$A_1 = \begin{bmatrix} 1 & 0 & -0.1v_{ref} \\ 0 & 1 & 0.1v_{ref} \\ 0 & 0 & 1 \end{bmatrix}, A_2 = \begin{bmatrix} 1 & 0 & 0.1v_{ref} \\ 0 & 1 & 0.1v_{ref} \\ 0 & 0 & 1 \end{bmatrix}$$

$$A_3 = \begin{bmatrix} 1 & 0 & -0.1v_{ref} \\ 0 & 1 & -0.1v_{ref} \\ 0 & 0 & 1 \end{bmatrix}, A_4 = \begin{bmatrix} 1 & 0 & 0.1v_{ref} \\ 0 & 1 & -0.1v_{ref} \\ 0 & 0 & 1 \end{bmatrix}$$

$$B_1 = \begin{bmatrix} -0.1 & 0 \\ 0.1 & 0 \\ 0.004 & 0.039v_{ref} \end{bmatrix}, B_2 = \begin{bmatrix} 0.1 & 0 \\ 0.1 & 0 \\ 0.004 & 0.039v_{ref} \end{bmatrix}$$

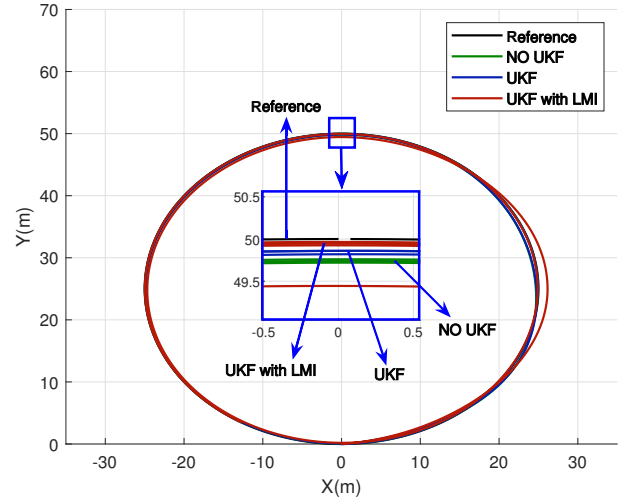
$$B_3 = \begin{bmatrix} 0.1 & 0 \\ -0.1 & 0 \\ 0.004 & 0.039v_{ref} \end{bmatrix}, B_4 = \begin{bmatrix} -0.1 & 0 \\ -0.1 & 0 \\ 0.004 & 0.039v_{ref} \end{bmatrix}$$

$$Q_c = \begin{bmatrix} 1 & 0 & 0 \\ 0 & 1 & 0 \\ 0 & 0 & 1 \end{bmatrix}, D_k = \begin{bmatrix} 1 & 0 & 0 \\ 0 & 1 & 0 \\ 0 & 0 & 0 \end{bmatrix}$$

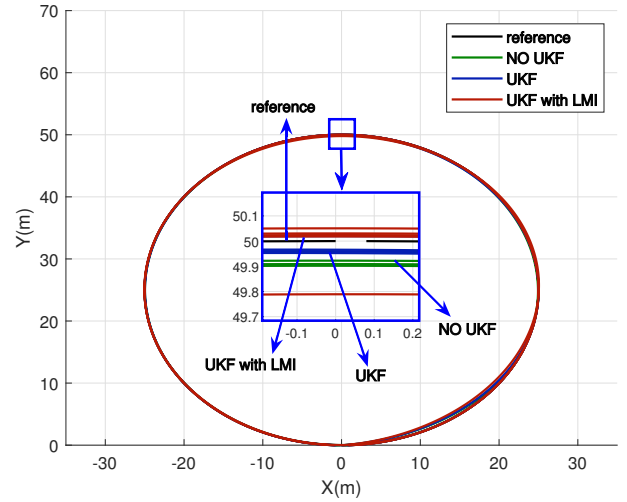
Define the remaining parameters of the simulation vehicle in accordance with the specifications outlined in [49]. Subsequently, three different methods are chosen for experimental simulation. Method A is the MPC method proposed in Section IV without filter. Method B is the MPC method proposed in Section IV with traditional UKF. Method C is the MPC method proposed in Section IV with LMI-constrained UKF.

Case 1: The starting point of the vehicle is within the reference trajectory

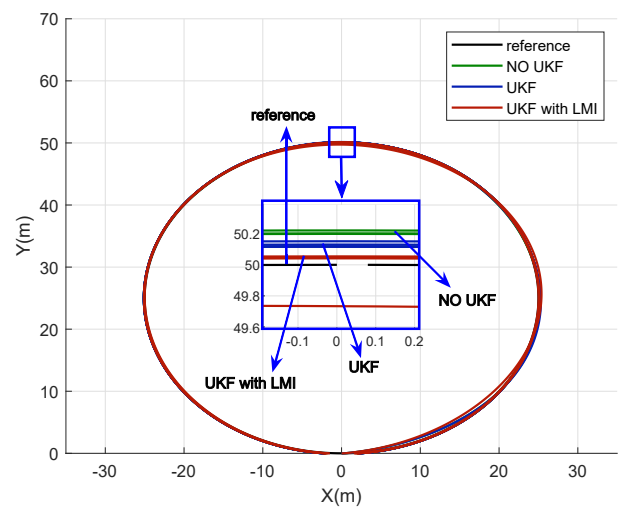
The starting point of the reference trajectory is $X_{ref}(0) = [0 \ 0 \ 0]^T$. The tracking ability of controller and the accuracy of estimation are evaluated by choosing different velocities in simulation. The speed v_{ref} is chosen as 3m/s, 5m/s and 8m/s, respectively. As shown in Fig. 5, the three methods all have good tracking performance at three speeds. Upon



(a) Trajectory tracking with different methods (3m/s)

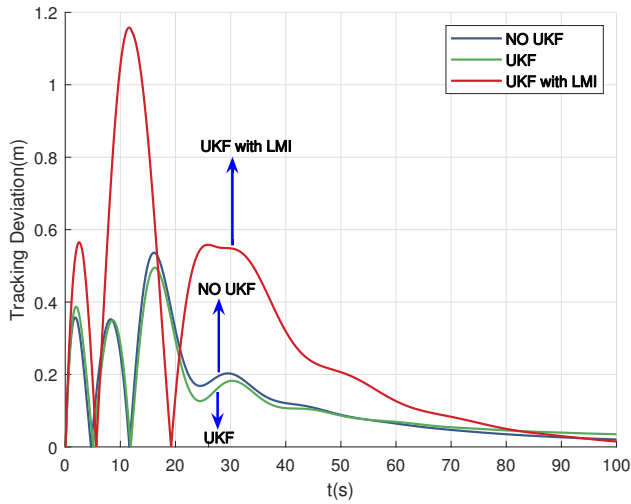


(b) Trajectory tracking with different methods (5m/s)

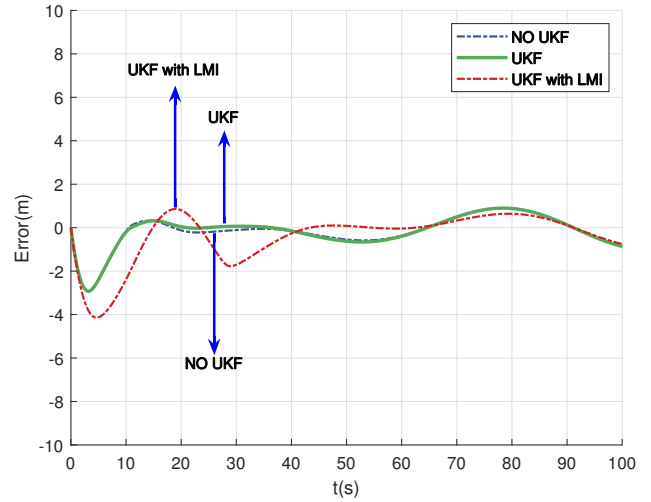


(c) Trajectory tracking with different methods (8m/s)

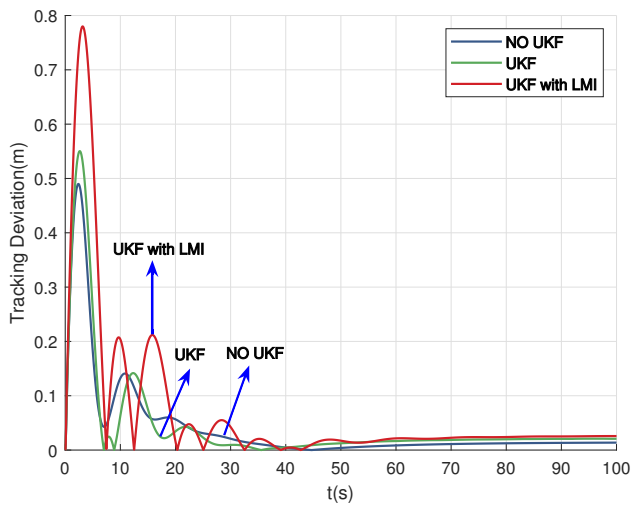
Fig. 5. Experimental simulation of vehicle trajectory tracking. The experiment was carried out in three different methods and at three different speeds at the starting point $X_{ref}(0) = [0 \ 0 \ 0]^T$.



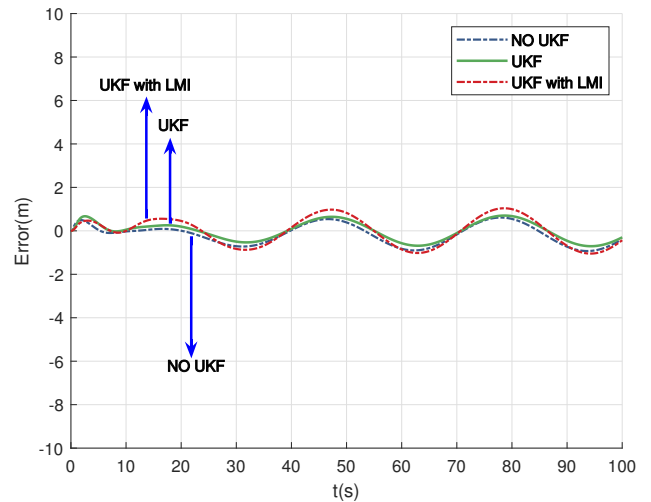
(a) Tracking deviation with different methods (3m/s)



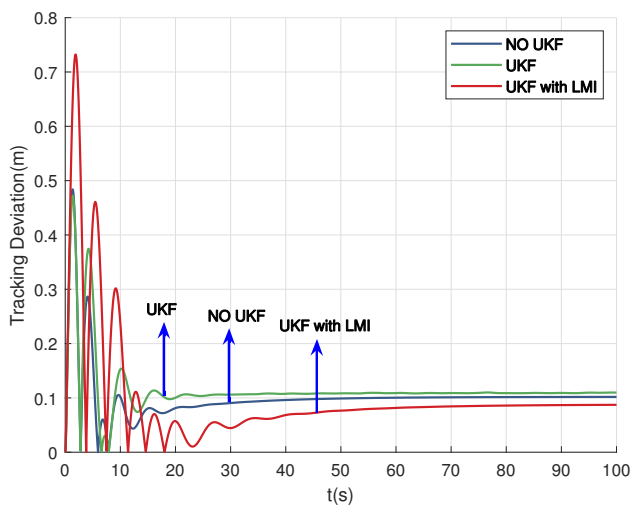
(a) X-direction deviation with different methods (3m/s)



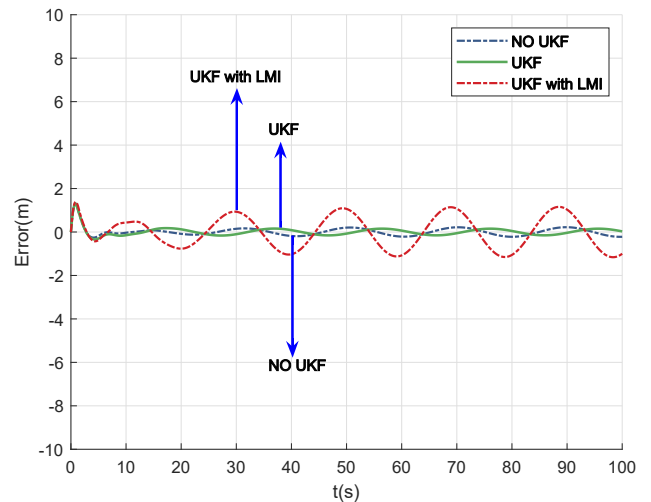
(b) Tracking deviation with different methods (5m/s)



(b) X-direction deviation with different methods (5m/s)



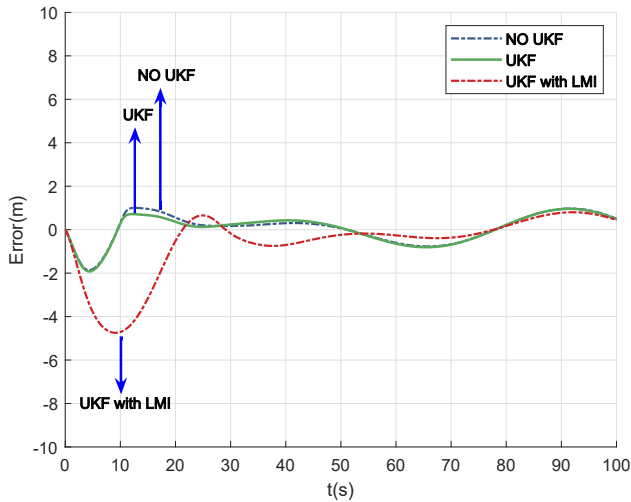
(c) Tracking deviation with different methods (8m/s)



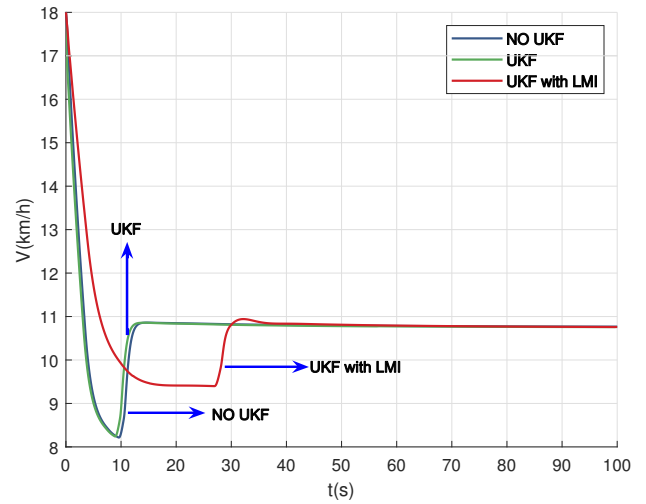
(c) X-direction deviation with different methods (8m/s)

Fig. 6. Tracking error between actual vehicle track and reference track at the starting point $X_{ref}(0) = [0 \ 0 \ 0]^T$.

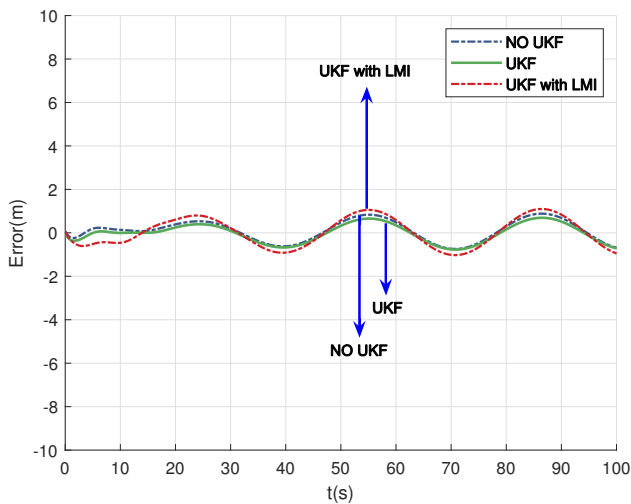
Fig. 7. The deviation of X-direction between actual vehicle track and reference track at the starting point $X_{ref}(0) = [0 \ 0 \ 0]^T$.



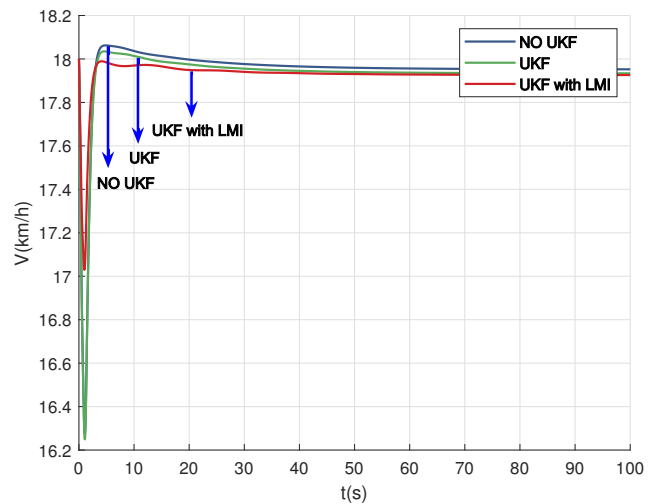
(a) Y-direction deviation with different methods (3m/s)



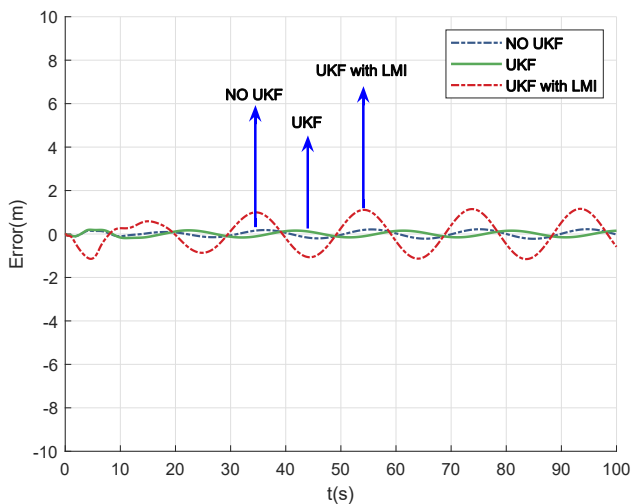
(a) Speed with different methods (3m/s)



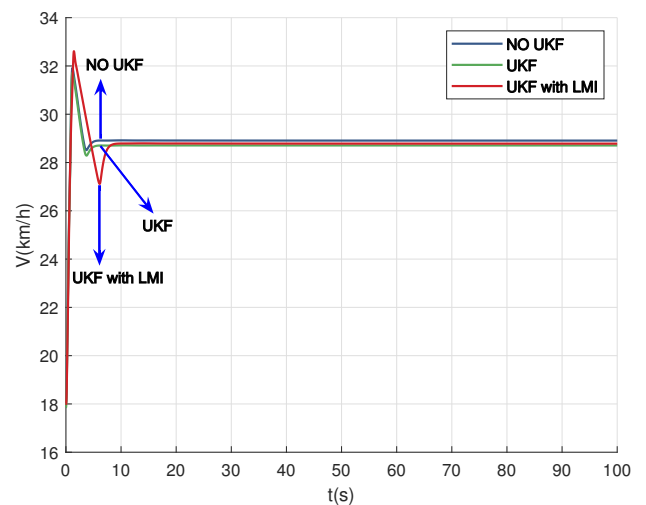
(b) Y-direction deviation with different methods (5m/s)



(b) Speed with different methods (5m/s)



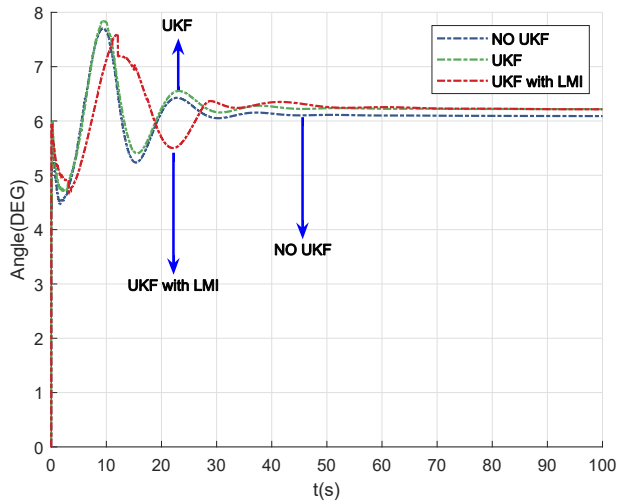
(c) Y-direction deviation with different methods (8m/s)



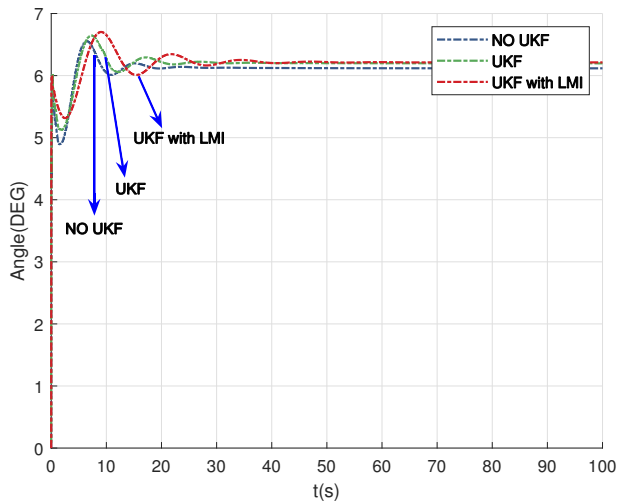
(c) Speed with different methods (8m/s)

Fig. 8. The deviation of Y-direction between actual vehicle track and reference track at the starting point $X_{ref}(0) = [0 \ 0 \ 0]^T$.

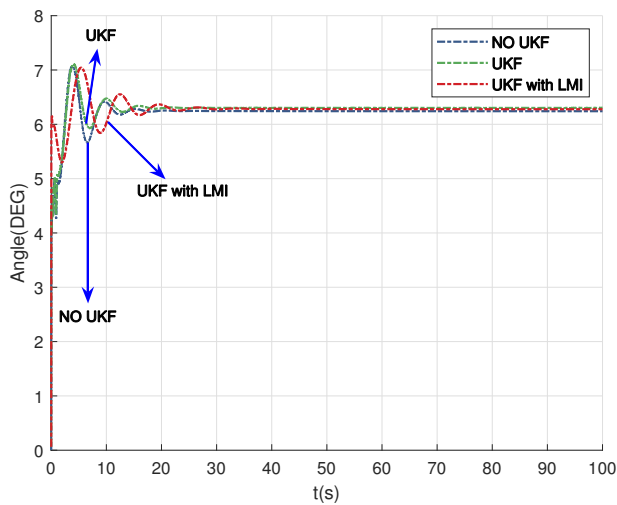
Fig. 9. The simulation of vehicle speed with different methods at the starting point $X_{ref}(0) = [0 \ 0 \ 0]^T$.



(a) Wheel steer with different methods (3m/s)

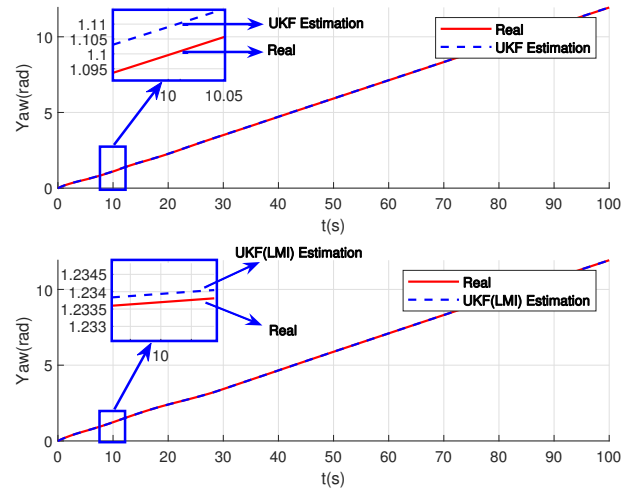


(b) Wheel steer with different methods (5m/s)

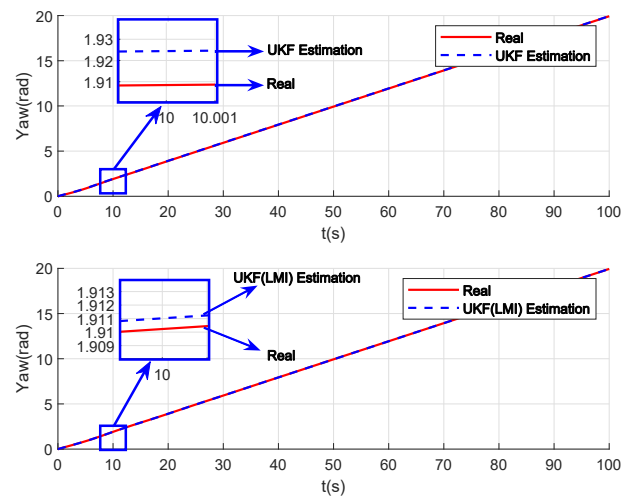


(c) Wheel steer with different methods (8m/s)

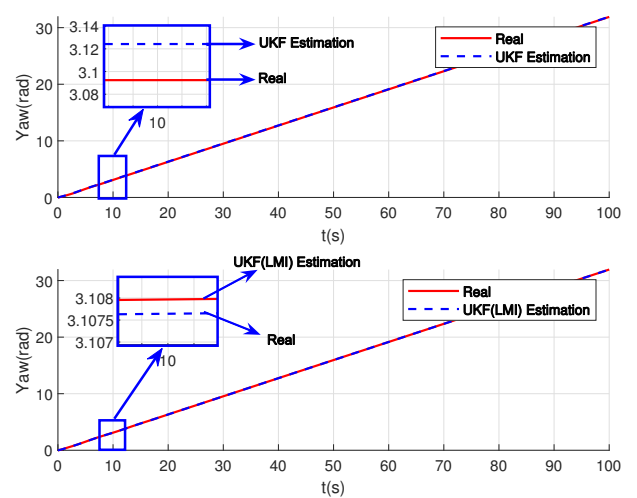
Fig. 10. The simulation of wheel steer with different methods at the starting point $X_{ref}(0) = [0 \ 0 \ 0]^T$.



(a) Yaw estimate with different methods (3m/s)

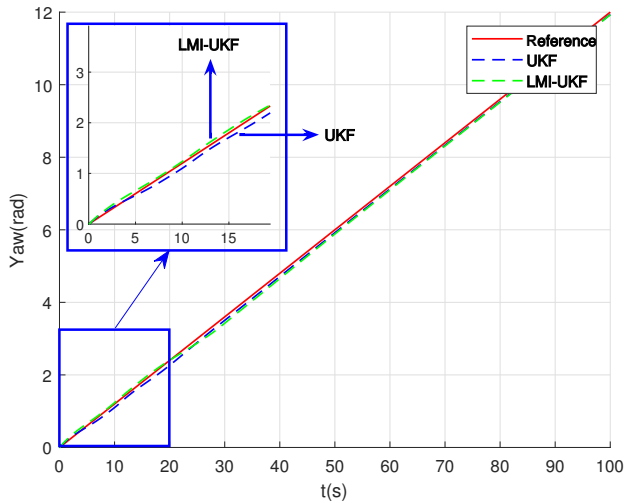


(b) Yaw estimate with different methods (5m/s)

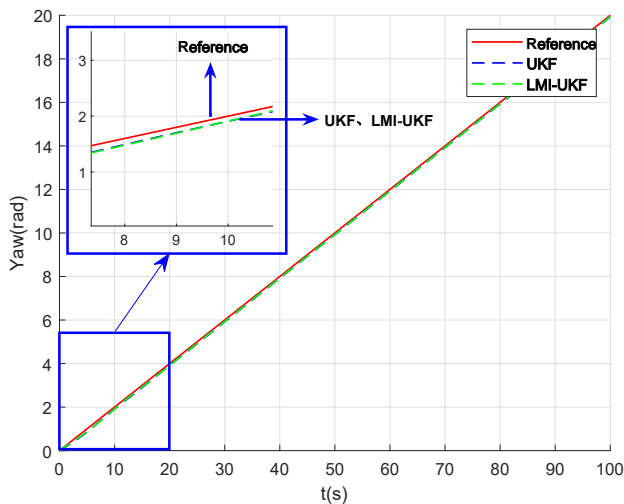


(c) Yaw estimate with different methods (8m/s)

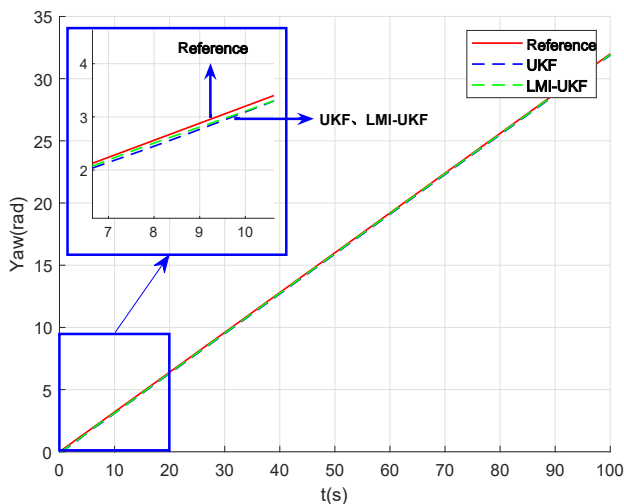
Fig. 11. The estimation of vehicle Yaw using both the UKF and the LMI-constrained UKF at the starting point $X_{ref}(0) = [0 \ 0 \ 0]^T$.



(a) Comparison of Yaw for UKF and LMI-constrained UKF (3m/s)



(b) Comparison of Yaw for UKF and LMI-constrained UKF (5m/s)



(c) Comparison of Yaw for UKF and LMI-constrained UKF (8m/s)

Fig. 12. The simulation of vehicle Yaw with traditional UKF and the LMI-Constrained UKF in this paper at the starting point $X_{ref}(0) = [0 \ 0 \ 0]^T$.

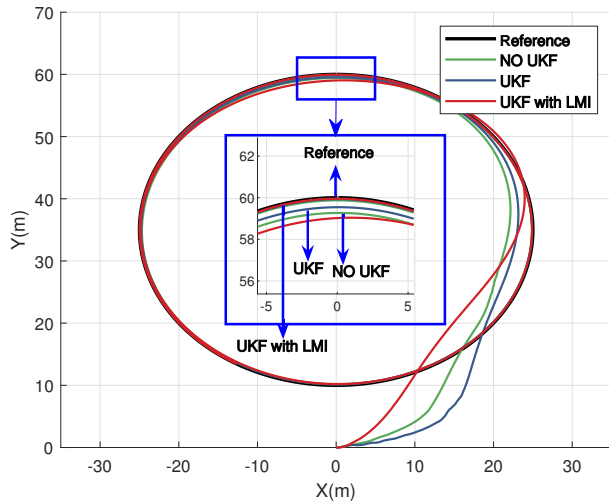
analysis of Fig. 6, Fig. 7, and Fig. 8, it is evident that the deviations resulting from the three methods are small, all less than 1m. However, as the speed increases to 8m/s, Method C demonstrates better performance. From this, it can be seen that when the starting point of the vehicle is on the reference trajectory, the requirements for the accuracy of vehicle state estimation and the robustness of MPC algorithm are not high, and the results obtained by the three methods are all excellent.

According to Fig. 9, the results indicate that the vehicle can reach the reference speed through three methods. Comparing with method A and method B, method C has smaller overshoot. Throughout the motion of the vehicle, the wheel angle plays a crucial role in influencing trajectory tracking performance, as depicted in Fig. 10. Under the action of method C, the downward overshoot of tire angle is smaller, which has a faster response speed and can adjust tire angle faster to achieve the purpose of tracking the reference trajectory. In Fig. 11, the results show that LMI-constrained UKF estimation error is smaller than traditional UKF estimation error at different speeds. In Fig. 12, the deviation between the vehicle yaw and the expected yaw under the action of method B and method C is similar.

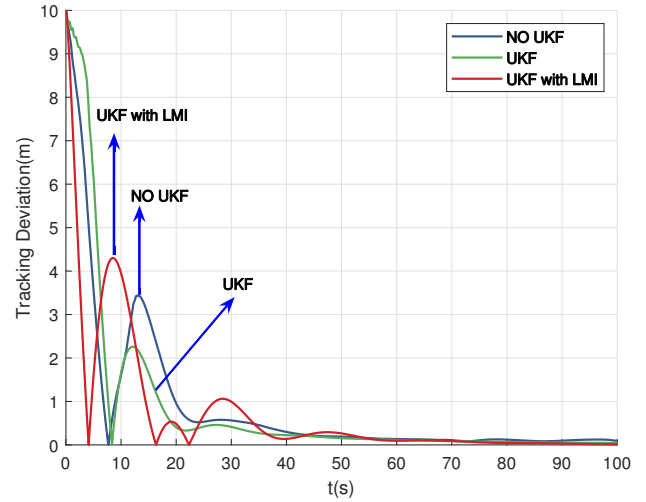
Case 2: The starting point of the vehicle is outside the reference trajectory

The starting point of the reference trajectory is $X_{ref}(0) = [0 \ 10 \ 0]^T$. The tracking ability of controller and the accuracy of estimation are evaluated by choosing different velocities in simulation. When the starting point of the vehicle is outside the reference trajectory, higher filtering accuracy and robustness of the MPC algorithm are required. As shown in Fig. 13, at speed of 3m/s and 5m/s, all three methods demonstrate good tracking performance. According to Figs. 13(a) and 13(b), method B and method C have better tracking performance than method A. The vehicle using method C approaches the reference trajectory more quickly and travels along the reference trajectory more closely. Fig. 13(c) shows that, at the speed of 8m/s, the three methods have a certain degree of fluctuation at the beginning of movement. The vehicle using Method A adheres to the reference trajectory after completing two laps, while the vehicle employing Method B needs one lap, and the vehicle utilizing Method C adheres the trajectory in just half a lap. The tracking error of the three methods have little difference at 3m/s and 5m/s speeds, as seen in Figs. 14(a), 14(b), 15 and 16, when speed increasing to 8m/s, method C shows better performance. In Fig. 14(c), the tracking error converges faster and fluctuates less.

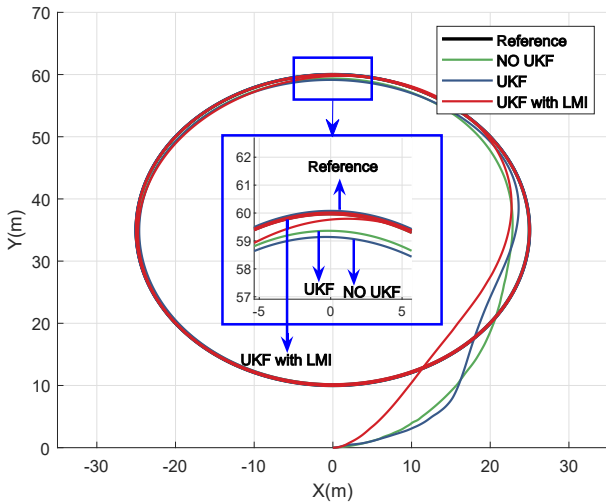
According to Fig. 17, the results indicate that the vehicle can reach the reference speed through three methods. At low speeds, the tracking convergence speeds of the three methods are comparable, as depicted in Fig. 17(a). The overshoot for both method A and method B increases significantly as the speed rises. Comparing with method A and method B, method C has faster convergence speed and smaller overshoot. During vehicle moving, the value of wheel angle will directly affect the performance of trajectory tracking, the results are shown in Fig. 18. At the speed of 8 m/s, the wheel angle under method C converges to the reference value within 20 seconds, which is faster than method A and method B. According to the definition in this paper, φ increases



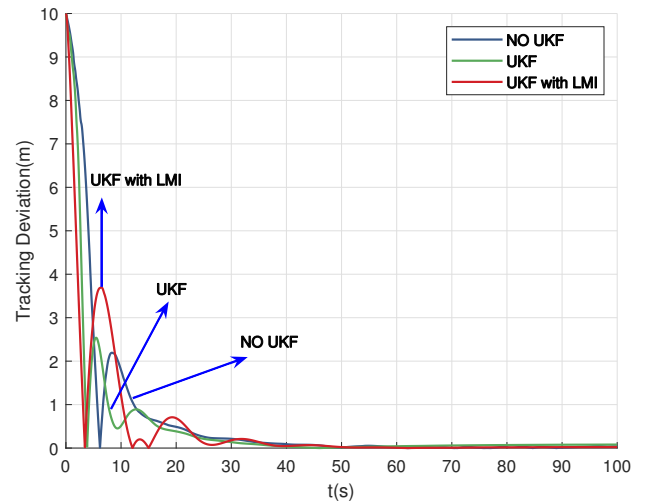
(a) Trajectory tracking with different methods (3m/s)



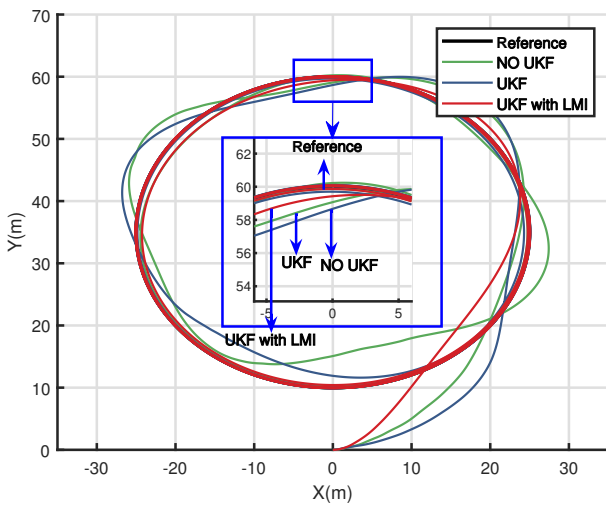
(a) Tracking deviation with different methods (3m/s)



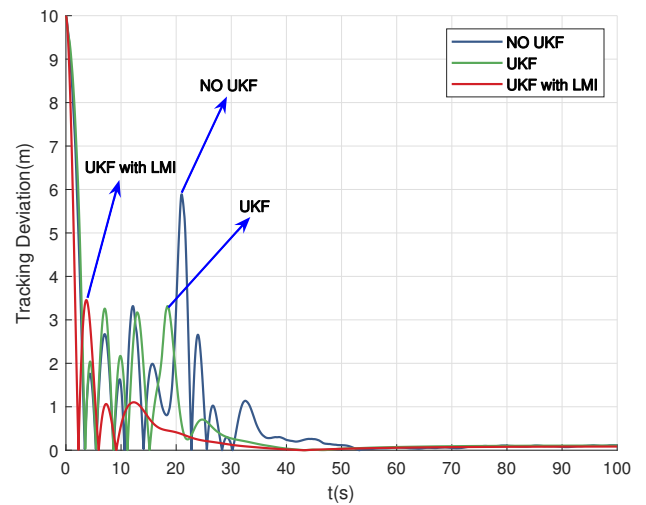
(b) Trajectory tracking with different methods (5m/s)



(b) Tracking deviation with different methods (5m/s)



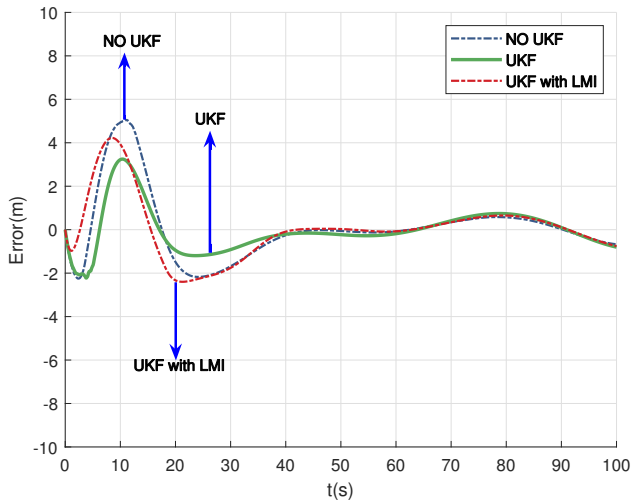
(c) Trajectory tracking with different methods (8m/s)



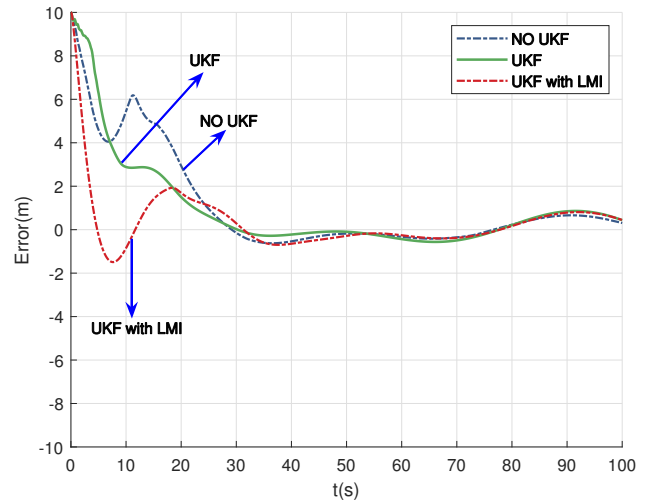
(c) Tracking deviation with different methods (8m/s)

Fig. 13. Experimental simulation of vehicle trajectory tracking. The experiment was carried out in three different methods and at three different speeds at the starting point $X_{ref}(0) = [0 \ 10 \ 0]^T$.

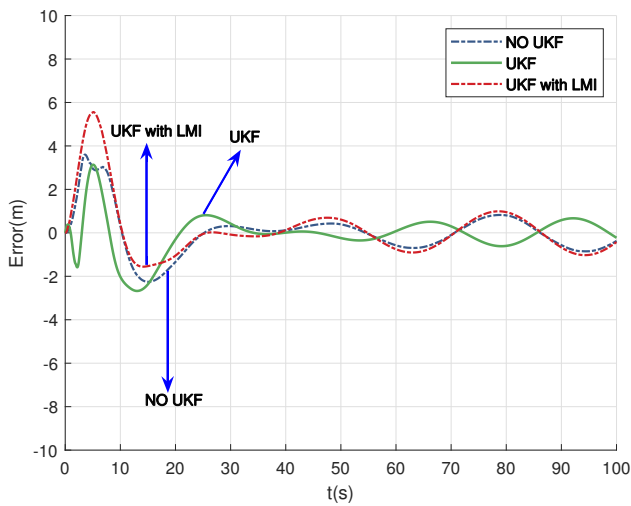
Fig. 14. Tracking error between actual vehicle track and reference track at the starting point $X_{ref}(0) = [0 \ 10 \ 0]^T$.



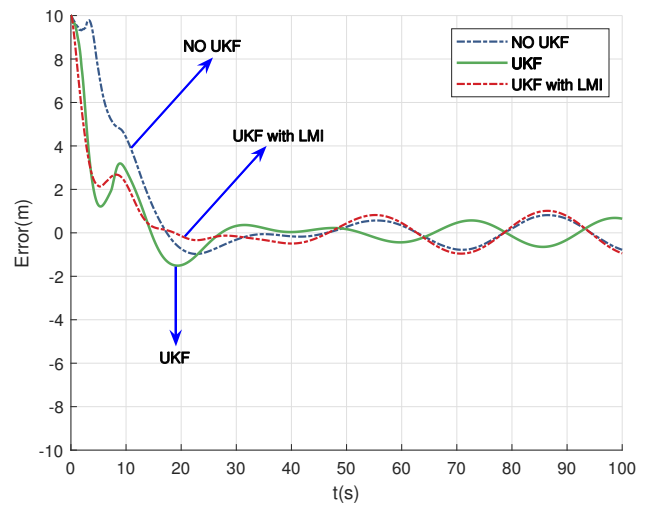
(a) X-direction deviation with different methods (3m/s)



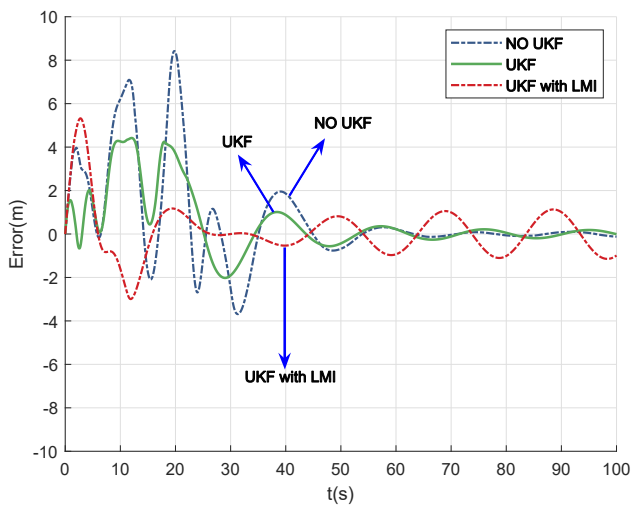
(a) Y-direction deviation with different methods (3m/s)



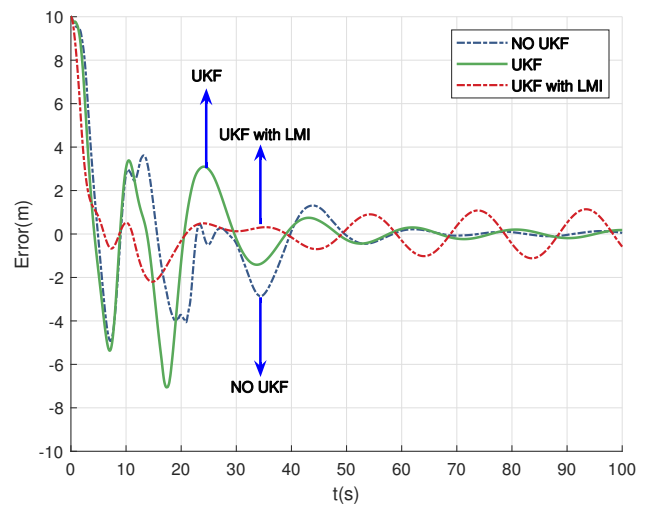
(b) X-direction deviation with different methods (5m/s)



(b) Y-direction deviation with different methods (5m/s)



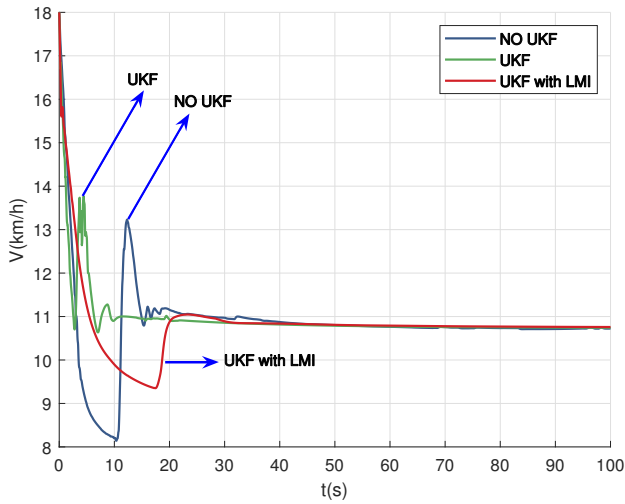
(c) X-direction deviation with different methods (8m/s)



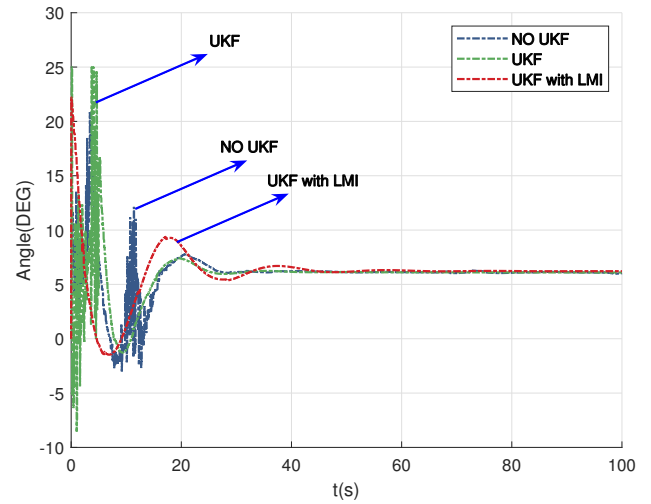
(c) Y-direction deviation with different methods (8m/s)

Fig. 15. The deviation of X-direction between actual vehicle track and reference track at the starting point $X_{ref}(0) = [0 \ 10 \ 0]^T$.

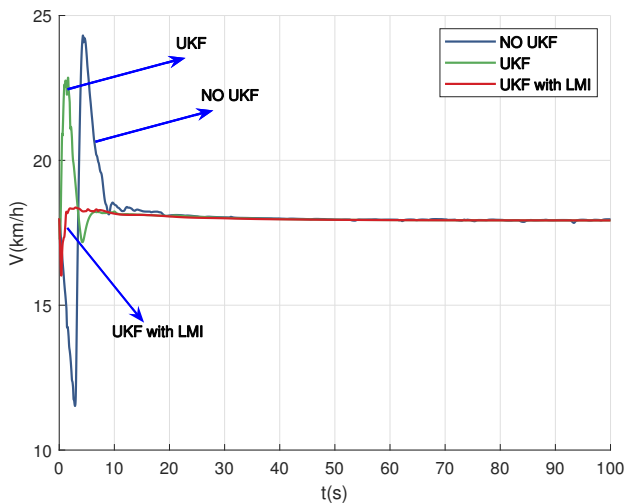
Fig. 16. The deviation of Y-direction between actual vehicle track and reference track at the starting point $X_{ref}(0) = [0 \ 10 \ 0]^T$.



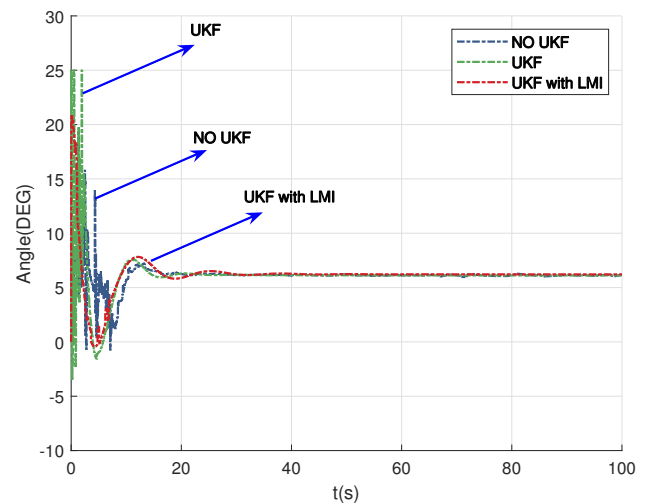
(a) Speed with different methods (3m/s)



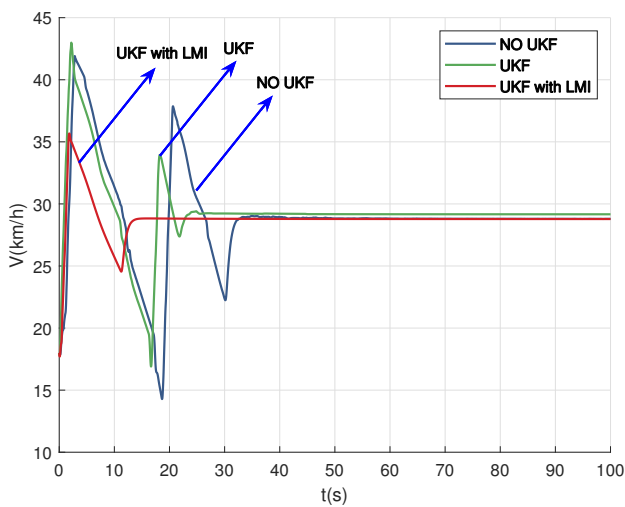
(a) Wheel steer with different methods (3m/s)



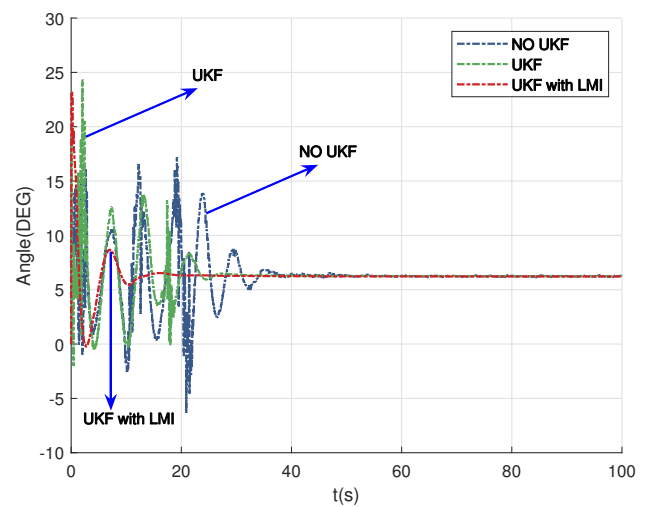
(b) Speed with different methods (5m/s)



(b) Wheel steer with different methods (5m/s)



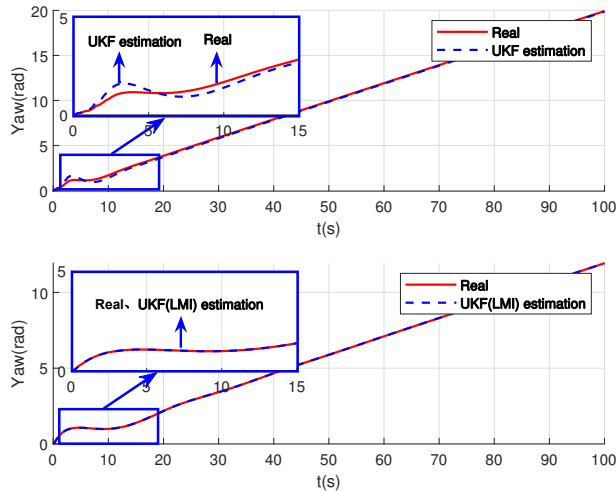
(c) Speed with different methods (8m/s)



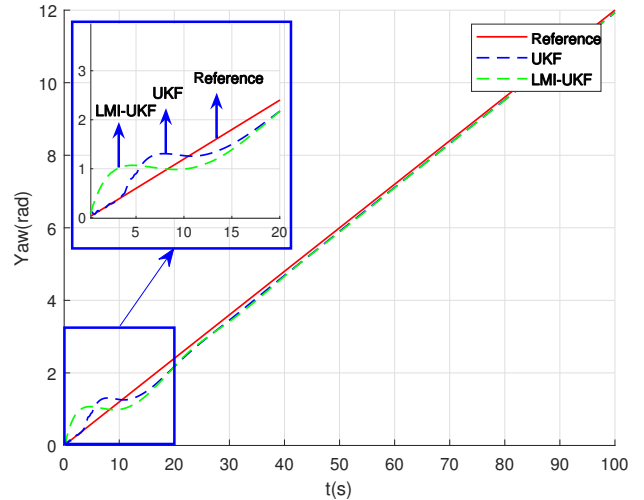
(c) Wheel steer with different methods (8m/s)

Fig. 17. The simulation of vehicle speed with different methods at the starting point $X_{ref}(0) = [0 \ 10 \ 0]^T$.

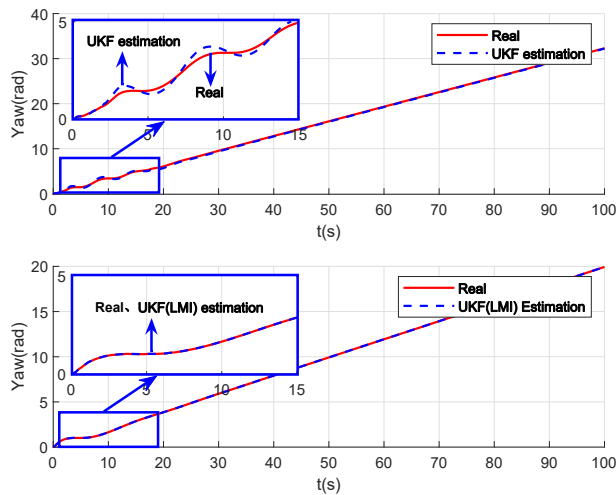
Fig. 18. The simulation of wheel steer with different methods at the starting point $X_{ref}(0) = [0 \ 10 \ 0]^T$.



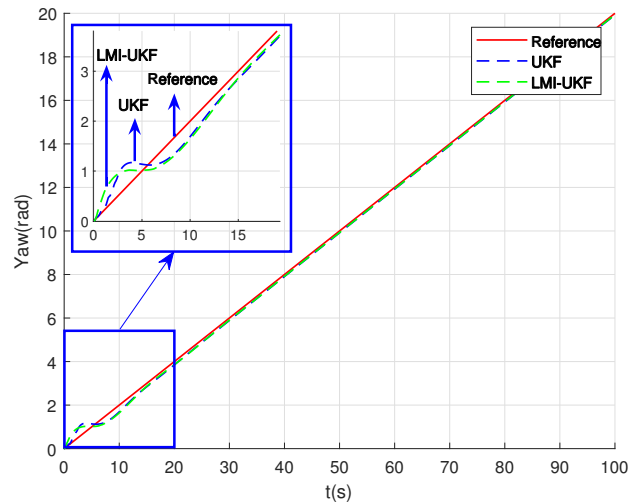
(a) Yaw estimate with different methods (3m/s)



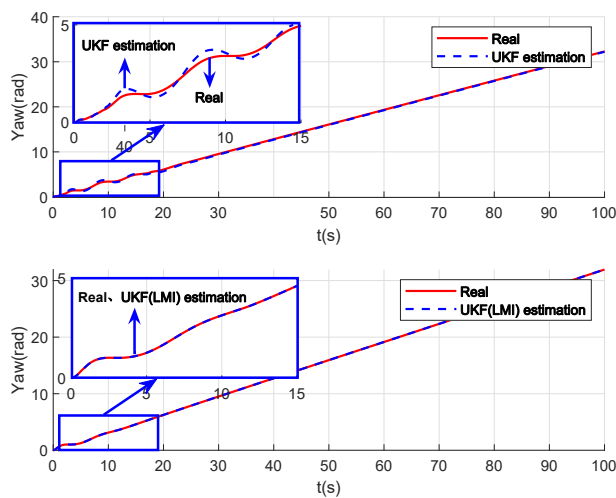
(a) Comparison of Yaw for UKF and LMI-constrained UKF (3m/s)



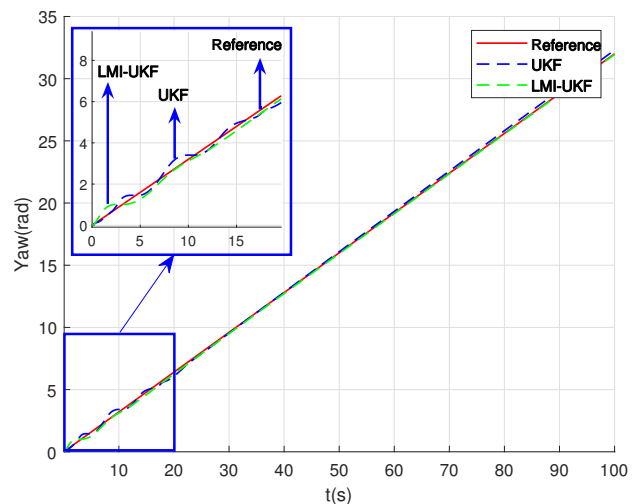
(b) Yaw estimate with different methods (5m/s)



(b) Comparison of Yaw for UKF and LMI-constrained UKF (5m/s)



(c) Yaw estimate with different methods (8m/s)



(c) Comparison of Yaw for UKF and LMI-constrained UKF (8m/s)

Fig. 19. The estimation of vehicle Yaw using both the UKF and the LMI-constrained UKF at the starting point $X_{ref}(0) = [0 \ 10 \ 0]^T$.

Fig. 20. The simulation of vehicle Yaw with traditional UKF and the LMI-Constrained UKF in this paper at the starting point $X_{ref}(0) = [0 \ 10 \ 0]^T$.

linearly with time. In Fig. 19, the results show that LMI-constrained UKF estimation error is smaller than traditional UKF estimation error at different speeds. From Fig. 20, it can be seen that the vehicle yaw under the action of LMI-constrained UKF can quickly track the expected yaw. method C has a better improvement on the vehicle than method B as the speed increases.

VI. CONCLUSIONS

In this paper, a nonlinear vehicle state estimation using LMI-constrained UKF method and a robust MPC with actuator saturation and disturbance for the problem of trajectory tracking are proposed. We use the co-simulation platform of MATLAB/Simulink and Carsim to verify the feasibility of the approach. The estimation of LMI-constrained UKF is more accurate than the estimation of UKF. The performance of the controller in Section IV is verified with three different methods. The method with a filter has better control performance than the method without a filter, and the result of method C is better. Furthermore, in our subsequent research, we plan to construct a physical platform to validate the proposed method. Additionally, our ongoing investigation aims to enhance the driving speed of unmanned vehicles while maintaining optimal control performance.

REFERENCES

- [1] M. Noorollahzadegan, A. Vali, G. Derakhshan, H. Arasteh Rad, and V. Behnamgol, "Design of a Robust Controller for an Unmanned Vehicle Based on Sliding Mode Theory," *Engineering Letters*, vol. 30, no. 2, pp. 875-881, 2022.
- [2] Binbin Sun, Wentao Li, Huibin Liu, Jinghao Yan, Song Gao, and Penghang Feng, "Obstacle Detection of Intelligent Vehicle Based on Fusion of Lidar and Machine Vision," *Engineering Letters*, vol. 29, no. 2, pp. 722-730, 2021.
- [3] Zhigang Zhou, Xinqing Ding, Zhichong Shi, Xiaofei Yin, and Xiangming Meng, "In-wheel Motor Electric Vehicle Based on Fuzzy Neural Network Yaw Stability Optimization Control," *Engineering Letters*, vol. 31, no. 4, pp. 1717-1723, 2023.
- [4] Chongyang Lv, Fei Yu, Minghong Zhu, and Shu Xiao, "AUV Real-time Dynamic Obstacle Avoidance Strategy Based on Relative Motion," *Engineering Letters*, vol. 27, no. 1, pp. 234-240, 2019.
- [5] I. Gokasar, A. Timurogullari, S. S. Ozkan, and M. Deveci, "IDILIM: Incident Detection Included Linear Management using Connected Autonomous Vehicles," *Annals of Operations Research*, pp. 1-20, 2023.
- [6] K. Suganthi, M. A. Kumar, N. Harish, S. HariKrishnan, G. Rajesh, and S. S. Reka, "Advanced Driver Assistance System Based on IoT V2V and V2I for Vision Enabled Lane Changing with Futuristic Drivability," *Sensors*, vol. 23, no. 7, p. 3423, 2023.
- [7] X. Zhang, Z. Fan, X. Tan, Q. Liu, and Y. Shi, "Spatiotemporal Adaptive Attention 3D Multiobject Tracking for Autonomous Driving," *Knowledge-Based Systems*, vol. 267, article. 110442, 2023.
- [8] Lie Yu, Lei Ding, and Yukang Tian, "Tracking Control for Intelligent Tracing Car based on Novel Path Tracking Strategy," *IAENG International Journal of Applied Mathematics*, vol. 53, no. 2, pp. 664-669, 2023.
- [9] Z. Jing, W. Huang, and H. Ma, "A Tracking Control Method for Collision Avoidance Trajectory of Autonomous Vehicle Based on Multi-Constraint MPC," *International Journal of Vehicle Design*, vol. 86, no. 1-4, pp. 106-123, 2021.
- [10] H. Pang, N. Liu, C. Hu, and Z. Xu, "A Practical Trajectory Tracking Control of Autonomous Vehicles Using Linear Time-varying MPC Method," *Proceedings of the Institution of Mechanical Engineers, Part D: Journal of Automobile Engineering*, vol. 236, no. 4, pp. 709-723, 2022.
- [11] T. Yuan and R. Zhao, "LQR-MPC-Based Trajectory-Tracking Controller of Autonomous Vehicle Subject to Coupling Effects and Driving State Uncertainties," *Sensors*, vol. 22, no. 15, p. 5556, 2022.
- [12] K. Zhang, Q. Sun, and Y. Shi, "Trajectory Tracking Control of Autonomous Ground Vehicles Using Adaptive Learning MPC," *IEEE Transactions on Neural Networks and Learning Systems*, vol. 32, no. 12, pp. 5554-5564, 2021.
- [13] G. Dean, "An Introduction to Kalman Filters," *Measurement and Control*, vol. 19, no. 2, pp. 69-73, 1986.
- [14] D. Marelli, M. Zamani, M. Fu, and B. Ninness, "Distributed Kalman Filter in a Network of Linear Systems," *Systems & Control Letters*, vol. 116, pp. 71-77, 2018.
- [15] D.-J. Xin and L.-F. Shi, "Kalman Filter for Linear Systems with Unknown Structural Parameters," *IEEE Transactions on Circuits and Systems II: Express Briefs*, vol. 69, no. 3, pp. 1852-1856, 2021.
- [16] D.-J. Xin and L.-F. Shi, "Intermediate-Variable-Based Kalman Filter for Linear Time-Varying Systems with Unknown Inputs," *International Journal of Robust and Nonlinear Control*, vol. 32, no. 4, pp. 2453-2464, 2022.
- [17] X. Yu, D. Xin, and J. Li, "Robust Kalman Filter for Linear System with Convex Polytopic Uncertainties," *IEEE Transactions on Circuits and Systems II: Express Briefs*, vol. 70, no. 2, pp. 821-825, 2022.
- [18] K. Shi, X. Wang, H. Xu, Z. Chen, and H. Zhao, "Integrated Approach to AUV Docking Based on Nonlinear Offset-Free Model Predictive Control," *Measurement and Control*, vol. 56, no. 3-4, pp. 733-750, 2023.
- [19] L. Tao, Y. Watanabe, and H. Takada, "A Lightweight Long-Term Vehicular Motion Prediction Method Leveraging Spatial Database and Kinematic Trajectory Data," *ISPRS International Journal of Geo-Information*, vol. 11, no. 9, p. 463, 2022.
- [20] W. Farag, "Bayesian Localization in Real-Time Using Probabilistic Maps and Unscented-Kalman-Filters," *Journal of Engineering Research*, vol. 10, no. 3A, 2022.
- [21] W. Farag, "Multiple Road-Objects Detection and Tracking for Autonomous Driving," *Journal of Engineering Research*, vol. 10, no. 1A, pp. 237-262, 2022.
- [22] S. Liang, M. Xie, S. Garg, G. Kaddoum, M. M. Hassan, and S. A. AlQahtani, "An Augmented SLAM Method with a Visual-Lidar-Equipped Unmanned Vehicle for Detecting Control Measures Against COVID-19," *Human-Centric Computing and Information Sciences*, vol. 13, no. 1, 2023.
- [23] T. A. Wenzel, K. Burnham, M. Blundell, and R. Williams, "Dual Extended Kalman Filter for Vehicle State and Parameter Estimation," *Vehicle System Dynamics*, vol. 44, no. 2, pp. 153-171, 2006.
- [24] M. C. Best, T. Gordon, and P. Dixon, "An Extended Adaptive Kalman Filter for Real-Time State Estimation of Vehicle Handling Dynamics," *Vehicle System Dynamics*, vol. 34, no. 1, pp. 57-75, 2000.
- [25] G. Guo and S. Zhao, "3D Multi-Object Tracking with Adaptive Cubature Kalman Filter for Autonomous Driving," *IEEE Transactions on Intelligent Vehicles*, vol. 8, no. 1, pp. 512-519, 2022.
- [26] H. Wei, Y. Huang, F. Hu, B. Zhao, Z. Guo, and R. Zhang, "Motion Estimation Using Region-Level Segmentation and Extended Kalman Filter for Autonomous Driving," *Remote Sensing*, vol. 13, no. 9, p. 1828, 2021.
- [27] K. Dai, B. Sun, G. Wu, S. Zhao, F. Ma, Y. Zhang, and J. Wu, "LiDAR-Based Sensor Fusion SLAM and Localization for Autonomous Driving Vehicles in Complex Scenarios," *Journal of Imaging*, vol. 9, no. 2, p. 52, 2023.
- [28] S. E. Samada, V. Puig, and F. Nejari, "Robust TS-ANFIS MPC of an Autonomous Racing Electrical Vehicle Considering the Battery State of Charge," *IEEE/ASME Transactions on Mechatronics*, vol. 28, no. 2, pp. 656-667, 2023.
- [29] Z. Zheng, S. Wang, B. Gong, E. Su, and H. Huang, "Study on Angle-Only Relative Navigation for Unmanned Aerial Vehicle Formation in GPS-Denied Environment," *Proceedings of the Institution of Mechanical Engineers, Part G: Journal of Aerospace Engineering*, vol. 237, no. 10, pp. 2252-2265, 2023.
- [30] E. Hashemi, A. Khajepour, N. Moshchuk, and S.-K. Chen, "Real-Time Road Bank Estimation with Disturbance Observers for Vehicle Control Systems," *IEEE Transactions on Control Systems Technology*, vol. 30, no. 1, pp. 443-450, 2021.
- [31] J. Hu, S. Rakheja, and Y. Zhang, "Tire-Road Friction Coefficient Estimation Based on Designed Braking Pressure Pulse," *Proceedings of the Institution of Mechanical Engineers, Part D: Journal of Automobile Engineering*, vol. 235, no. 7, pp. 1876-1891, 2021.
- [32] R. Cen, T. Jiang, Y. Tan, X. Su, and F. Xue, "A Low-Cost Visual Inertial Odometry for Mobile Vehicle Based on Double Stage Kalman Filter," *Signal Processing*, vol. 197, article. 108537, 2022.
- [33] D. Gabriel, D. Baumgärtner, and D. Görge, "Accurate and Robust State Estimation for Bicycles," *Vehicle System Dynamics*, vol. 61, no. 9, pp. 2338-2351, 2022.
- [34] E. Hrustic, R. Ben Abdallah, J. Vilà-Valls, D. Vivet, G. Pagès, and E. Chaumette, "Robust Linearly Constrained Extended Kalman Filter for Mismatched Nonlinear Systems," *International Journal of Robust and Nonlinear Control*, vol. 31, no. 3, pp. 787-805, 2021.
- [35] H. Guo, D. Cao, H. Chen, Z. Sun, and Y. Hu, "Model Predictive Path Following Control for Autonomous Cars Considering a Measurable Disturbance: Implementation, Testing, and Verification," *Mechanical*

- Systems and Signal Processing*, vol. 118, pp. 41-60, 2019.
- [36] J. Hu, S. Xiong, J. Zha, and C. Fu, "Lane Detection and Trajectory Tracking Control of Autonomous Vehicle Based on Model Predictive Control," *International Journal of Automotive Technology*, vol. 21, pp. 285-295, 2020.
- [37] T. M. Vu, R. Moezzi, J. Cyrus, and J. Hlava, "Model Predictive Control for Autonomous Driving Vehicles," *Electronics*, vol. 10, no. 21, p. 2593, 2021.
- [38] H. Peng, W. Wang, Q. An, C. Xiang, and L. Li, "Path Tracking and Direct Yaw Moment Coordinated Control Based on Robust MPC with the Finite Time Horizon for Autonomous Independent-Drive Vehicles," *IEEE Transactions on Vehicular Technology*, vol. 69, no. 6, pp. 6053-6066, 2020.
- [39] J. Song, G. Tao, Z. Zang, H. Dong, B. Wang, and J. Gong, "Isolating Trajectory Tracking From Motion Control: A Model Predictive Control and Robust Control Framework for Unmanned Ground Vehicles," *IEEE Robotics and Automation Letters*, vol. 8, no. 3, pp. 1699-1706, 2023.
- [40] M. Cai, Y. Wang, S. Wang, R. Wang, and M. Tan, "Autonomous Manipulation of an Underwater Vehicle-Manipulator System by a Composite Control Scheme With Disturbance Estimation," *IEEE Transactions on Automation Science and Engineering*, vol. 21, no. 1, pp. 1012-1022, 2024.
- [41] M. Yue, C. An, and Z. Li, "Constrained Adaptive Robust Trajectory Tracking for WIP Vehicles Using Model Predictive Control and Extended State Observer," *IEEE Transactions on Systems, Man, and Cybernetics: Systems*, vol. 48, no. 5, pp. 733-742, 2016.
- [42] Q. Cui, R. Ding, B. Zhou, and X. Wu, "Path-Tracking of an Autonomous Vehicle via Model Predictive Control and Nonlinear Filtering," *Proceedings of the Institution of Mechanical Engineers, Part D: Journal of Automobile Engineering*, vol. 232, no. 9, pp. 1237-1252, 2018.
- [43] H. Yu, J. Duan, S. Taheri, H. Cheng, and Z. Qi, "A Model Predictive Control Approach Combined Unscented Kalman Filter Vehicle State Estimation in Intelligent Vehicle Trajectory Tracking," *Advances in Mechanical Engineering*, vol. 7, no. 5, 2015.
- [44] J. Gong, Y. Jiang, and W. Xu, "Model Predictive Control for Autonomous Vehicles," *Beijing: Beijing Institute of Technology Press, Chap.* pp. 18-77, 2014.
- [45] R. Aucoin, S. A. Chee, and J. R. Forbes, "Linear-and Linear-Matrix-Inequality-Constrained State Estimation for Nonlinear Systems," *IEEE Transactions on Aerospace and Electronic Systems*, vol. 55, no. 6, pp. 3153-3167, 2019.
- [46] T. Hu, Z. Lin, and B. M. Chen, "An Analysis and Design Method for Linear Systems Subject to Actuator Saturation and Disturbance," *Automatica*, vol. 38, no. 2, pp. 351-359, 2002.
- [47] X. Tang, Z. Xia, and N. Wei, "On Designing the Hybrid-Triggered Dynamic Output Feedback Guaranteed Cost Control for Uncertain TS Fuzzy Networked Control Systems with Cyber Attack and Actuator Saturation," *Journal of the Franklin Institute*, vol. 359, no. 12, pp. 6196-6221, 2022.
- [48] X. Tang, L. Deng, and H. Qu, "Predictive Control for Networked Interval Type-2 T-S Fuzzy System via an Event-Triggered Dynamic Output Feedback Scheme," *IEEE Transactions on Fuzzy Systems*, vol. 27, no. 8, pp. 1573-1586, 2018.
- [49] R. Li, L. Zhang, and J. Wang, "A Control Method of Unmanned Car Following Under Time-Varying Relative Distance and Angle," *Acta Automatica Sinica*, vol. 48, no. 11, pp. 2031-2040, 2018.